

Published in final edited form as:

*Cell Calcium*. 2008 February ; 43(2): 122–141. doi:10.1016/j.ceca.2007.04.012.

## Sub-plasmalemmal $[Ca^{2+}]_i$ upstroke in myocytes of the guinea-pig small intestine evoked by muscarinic stimulation: $IP_3R$ -mediated $Ca^{2+}$ release induced by voltage-gated $Ca^{2+}$ entry

D.V. Gordienko<sup>a,b,\*</sup>, M.I. Harhun<sup>a</sup>, M.V. Kustov<sup>b</sup>, V. Pucovský<sup>a</sup>, and T.B. Bolton<sup>a</sup>

<sup>a</sup> Division of Basic Medical Sciences, Ion Channels and Cell Signalling Centre, St. George's University of London, Cranmer Terrace, London SW17 0RE, UK

<sup>b</sup> Laboratory of Molecular Pharmacology and Biophysics of Cell Signalling, Bogomoletz Institute of Physiology, 4 Bogomoletz str., Kiev-024, Ukraine

### Abstract

Membrane depolarization triggers  $Ca^{2+}$  release from the sarcoplasmic reticulum (SR) in skeletal muscles via direct interaction between the voltage-gated L-type  $Ca^{2+}$  channels (the dihydropyridine receptors; VGCCs) and ryanodine receptors (RyRs), while in cardiac muscles  $Ca^{2+}$  entry through VGCCs triggers RyR-mediated  $Ca^{2+}$  release via a  $Ca^{2+}$ -induced  $Ca^{2+}$ -release (CICR) mechanism. Here we demonstrate that in phasic smooth muscle of the guinea-pig small intestine, excitation evoked by muscarinic receptor activation triggers an abrupt  $Ca^{2+}$  release from sub-plasmalemmal (sub-PM) SR elements enriched with inositol 1,4,5-trisphosphate receptors ( $IP_3Rs$ ) and poor in RyRs. This was followed by a lesser rise, or oscillations in  $[Ca^{2+}]_i$ . The initial abrupt sub-PM  $[Ca^{2+}]_i$  upstroke was all but abolished by block of VGCCs (by 5  $\mu M$  nifedipine), depletion of intracellular  $Ca^{2+}$  stores (with 10  $\mu M$  cyclopiazonic acid) or inhibition of  $IP_3Rs$  (by 2  $\mu M$  xestospongine C or 30  $\mu M$  2-APB), but was not affected by block of RyRs (by 50 – 100  $\mu M$  tetracaine or 100  $\mu M$  ryanodine). Inhibition of either  $IP_3Rs$  or RyRs attenuated phasic muscarinic contraction by 73 %. Thus, in contrast to cardiac muscles, excitation-contraction coupling in this phasic visceral smooth muscle occurs by  $Ca^{2+}$  entry through VGCCs which evokes an initial  $IP_3R$ -mediated  $Ca^{2+}$  release activated via a CICR mechanism.

### 1. Introduction

Smooth muscle cells (SMCs) are stimulated to contract either by depolarization of the cell membrane (electromechanical coupling), often in the form of an action potential (AP), or by activation of a variety of receptors (pharmacomechanical coupling) usually coupled to G-proteins, or by a combination of these mechanisms [1]. Most smooth muscles exhibit voltage-gated  $Ca^{2+}$  channels (VGCCs) which are often manifest in the generation of APs, although in many vascular smooth muscles  $Ca^{2+}$  is believed to 'leak' into the cell through these VGCCs giving rise to 'sparklets' [2, 3]. The entry of  $Ca^{2+}$  into the SMC through VGCCs and by reverse  $Na^+/Ca^{2+}$  exchange [4] is believed to load the  $Ca^{2+}$  stores largely in the sarcoplasmic reticulum (SR). From here  $Ca^{2+}$  can be released either by a process of  $Ca^{2+}$ -induced  $Ca^{2+}$  release (CICR) through ryanodine receptors (RyRs) upon  $Ca^{2+}$  entry during an AP [5] or by the action of inositol 1,4,5 trisphosphate ( $IP_3$ ) generated by a  $G_{q/11}$ -link from an activated stimulant receptor to phospholipase C. The entry of  $Ca^{2+}$  through

\* Correspondence to Dr. D.V. Gordienko at Division of Basic Medical Sciences, Ion Channels and Cell Signalling Centre, St. George's University of London, Cranmer Terrace, London SW17 0RE, UK. Tel: 020 8725 5657, Fax: 020 8275 3581, e-mail: gordienk@sgul.ac.uk.

VGCCs is believed to load SR calcium stores which, upon reaching a critical level of loading [6] discharge packets of  $\text{Ca}^{2+}$  which in the majority of smooth muscles generate transient high local concentrations of sub-PM  $\text{Ca}^{2+}$  that open  $\text{Ca}^{2+}$ -dependent potassium (BK) channels, present in abundance in the cell membrane of smooth muscles. Bursts of openings of these BK channels are seen as spontaneous transient outward currents (STOCs) in voltage-clamped SMCs [7-9]. In vascular smooth muscles loaded with a fluorescent  $\text{Ca}^{2+}$  indicator, the transient localised sub-plasmalemmal (sub-PM) increase in  $\text{Ca}^{2+}$  concentration ( $[\text{Ca}^{2+}]_i$ ) is seen as a flash of emitted light (“spark”, [10, 11]). The transient BK channel currents evoked have been observed to hyperpolarize the membrane so reducing  $\text{Ca}^{2+}$  entry through VGCCs, reducing the rate of  $\text{Ca}^{2+}$  loading of the SR stores, and so reducing tension [11, 12]. It seems that  $\text{Ca}^{2+}$  sparks are a negative feed-back mechanism, triggered by store overload, which regulate vascular myocyte tension as they barely increase global  $[\text{Ca}^{2+}]_i$ , while the high local sub-PM  $[\text{Ca}^{2+}]_i$  they create trigger a membrane-potential dependent relaxation of tension through the opening of BK channels [13].

The respective role of SR RyRs and  $\text{IP}_3$  receptors ( $\text{IP}_3\text{Rs}$ ) in the generation of smooth muscle myocyte tension is an area of active investigation. As smooth muscles do not have a sarcomeric organisation of their contractile proteins and calcium stores, the sites of  $\text{Ca}^{2+}$  release and re-storage are necessarily very different from those of striated muscles. In vas deferens and bladder SMCs an AP generates  $\text{Ca}^{2+}$  release from sub-PM ‘hot spots’ which then generate a cell-wide  $\text{Ca}^{2+}$  wave presumably by CICR. This is followed by SMC contraction [5]. Activation of stimulant receptors, such as muscarinic receptors in intestinal SMCs, triggers additional spark activity at spontaneously discharging ‘frequent discharge sites’ and recruits additional spark discharge sites [14]. The role of  $\text{IP}_3\text{Rs}$  seems to be to facilitate CICR within and between RyRs domains [15-18]. In colonic SMCs  $\text{IP}_3\text{R}$ -evoked  $\text{Ca}^{2+}$  release did not activate RyRs but RyR blockers inhibited  $\text{IP}_3\text{R}$ -mediated  $\text{Ca}^{2+}$  signals [19]. In vascular SMCs of small arteries Lamont and Wier [20] concluded that if RyRs were blocked, cell-wide  $\text{Ca}^{2+}$  waves could still be evoked by strong activation of adrenoceptors leading to myocyte and vessel contraction; thus CICR release apparently can occur among  $\text{IP}_3\text{Rs}$  alone although normally, at low levels of adrenoceptor activation RyRs were necessary to trigger  $\text{IP}_3\text{R}$  dependent  $\text{Ca}^{2+}$  waves [12]. Thus at physiologically important levels of tension the interplay of RyR and  $\text{IP}_3\text{R}$   $\text{Ca}^{2+}$  release is important as in visceral smooth muscles. The present work examines the relative roles of RyRs,  $\text{IP}_3\text{Rs}$  and VGCCs in intracellular  $\text{Ca}^{2+}$  mobilisation in longitudinal intestinal smooth muscle myocytes in response to strong activation of muscarinic receptors. A preliminary account of some of this work has previously been published in an abstract form [21].

## 2. Materials and methods

Experiments were performed on preparations of the longitudinal muscle layer of the guinea-pig ileum: (1) freshly isolated SMCs or (2) freshly dissected strips of smooth muscles (see below). Adult male guinea-pigs (300 – 500 g) were killed by decapitation after cervical dislocation as approved under Schedule 1 of the UK Animals (Scientific Procedures) Act 1986.

### 2.1. Cell preparation

The longitudinal muscle layer of the ileum was dissected and cut into small pieces, which were placed in  $\text{Ca}^{2+}$ - free physiological saline solution (PSS, see below). The pieces of the tissue were transferred into the same solution supplemented with (mg/ml): protease (Type X) 0.5, collagenase (Type 1A) 1.5, soybean trypsin inhibitor 1 and bovine serum albumin 1, and incubated for 20 min at 37 °C. The pieces of the tissue were then rinsed for 10 min in an enzyme-free  $\text{Ca}^{2+}$ - free solution and triturated with a wide bore glass pipette. Small aliquots of the cell suspension were transferred to the experimental chambers and diluted with PSS

composed of (mM): NaCl 120, KCl 6, CaCl<sub>2</sub> 2.5, MgCl<sub>2</sub> 1.2, glucose 12, HEPES 10; pH adjusted to 7.4 with NaOH. Experiments on isolated cells were conducted at 22 – 24 °C within 8 h of cell isolation.

## 2.2. Isometric tension recording

Smooth muscle strips (~10 mm in length) were dissected from longitudinal layer of guinea-pig ileum, transferred to a home-made organ bath (3 ml volume) and attached to an isometric force transducer at a resting tension load of 5 mN and bathed in the PSS at 37°C. The output of the force transducer was connected to a custom-made amplifier. The signals were digitized using a Digidata 1320 AD/DA converter (Molecular Devices Co., CA, USA) hosted by a PC running Axoscope 8.0 software (Molecular Devices Co., CA, USA).

## 2.3. Visualisation of [Ca<sup>2+</sup>]<sub>i</sub> changes

Changes in intracellular concentration of ionised calcium ([Ca<sup>2+</sup>]<sub>i</sub>) in isolated SMCs were imaged using the high-affinity ( $k_{d(Ca)} = 345$  nM) fluorescent Ca<sup>2+</sup> indicator fluo-4, which was loaded by 20-min incubation of the SMCs with 5 μM fluo-4 acetoxymethyl ester (fluo-4 AM) followed by a 40-min wash in PSS to allow time for de-esterification. To minimise SMC contraction, 40 μM of wortmannin was added to the bathing solution 10 min before imaging commenced.

The myocytes were stimulated with 10 μM carbachol (CCh) which was either superfused through the experimental bath or applied as a brief (~600 ms) pulse through a glass micropipette (located within 100 – 200 μm of the cell) attached to the outlet of pressure ejector Picospritzer III (Intracel Ltd., UK). Similar application of the control solution (without agonist) had no effect on [Ca<sup>2+</sup>]<sub>i</sub>. In the experiments where the same SMC was stimulated with CCh and caffeine, CCh was superfused through the experimental bath, while 5 mM caffeine was applied through a glass micropipette. Small volumes of antagonists were added to the bath solution in amounts calculated to achieve the indicated concentrations.

In the figures the intensity of fluo-4 fluorescence was normalised to the average fluorescence intensity in the images captured before CCh application and colour coded as indicated by the bars (F/F<sub>0</sub>). The temporal profiles of CCh-induced [Ca<sup>2+</sup>]<sub>i</sub> mobilisation are illustrated by the plots showing (1) the time course of the normalised fluo-4 fluorescence intensity (F/F<sub>0</sub>) averaged within multiple sub-PM regions (outlined in the corresponding images) where F/F<sub>0</sub> changes were initiated and rose above 2.5 or (2) the time course of F/F<sub>0</sub> averaged within entire confocal optical slice.

## 2.4. Visualisation of intracellular calcium stores

Distribution of intracellular calcium stores within isolated SMCs was visualised using the low-affinity ( $k_{d(Ca)} = 42$  μM) fluorescent Ca<sup>2+</sup> indicator fluo-3FF, which was loaded by 90-min incubation of the SMCs with 5 μM fluo-3FF AM followed by 60-min wash in PSS.

## 2.5. Immunostaining of RyRs and IP<sub>3</sub>Rs

Isolated SMCs were fixed by 5-10-min incubation with 4 % (w/v) paraformaldehyde. Nonspecific binding was blocked by incubating the SMCs with 3% (w/v) bovine serum albumin (BSA) and 0.3 % (w/v) Triton X-100 (a cell permeabilising agent) for 1 h at room temperature. Primary and secondary antibodies were diluted in PSS supplemented with 3% (w/v) BSA, 0.3 % (w/v) Triton X-100, 20 U/ml penicillin and 20 μg/ml streptomycin. To visualise the distribution of IP<sub>3</sub>Rs, we used an IP<sub>3</sub>R type 1 - specific antibody, since type 1 IP<sub>3</sub>R was shown to be ubiquitous in various tissues [22]. This antibody was developed (Sigma-Aldrich Co., RBI, Natick, MA, USA) in rabbit and has been shown to selectively recognise type 1 IP<sub>3</sub>Rs in other types of SMCs [23]. RyRs were detected with a monoclonal

anti-RyR antibody derived (Sigma-Aldrich Co., RBI, Natick, MA, USA) from the 34C hybridoma (produced by the fusion of P3X 63 Ag8.653 myeloma cells and spleen cells from Balb/c mice). This antibody reacts strongly with RyR type 1, type 2 and type 3. The SMCs were incubated in the presence of the primary anti-IP<sub>3</sub>R type 1 and anti-RyR antibodies (at 1:300 and 1:480 dilution, respectively) for 16 h at 4°C. Following a 10-min rinse (4 times) in PSS supplemented with 3% (w/v) BSA, primary antibody-specific binding was visualised by incubating SMCs for 2 h at room temperature with Alexa Fluor 488 conjugated to chicken anti-rabbit IgG (1:300 dilution, Invitrogen Ltd., UK) and Alexa Fluor 633 conjugated to goat anti-mouse IgG (1:300 dilution, Invitrogen Ltd., UK). In controls, primary antibodies were omitted from the experimental media during the first (16 h) incubation.

## 2.6. Confocal microscopy

Experimental chambers were placed on the stage of an Axiovert 100M inverted microscope attached to a LSM 510 laser-scanning unit (Zeiss, Oberkochen, Germany). The *x-y* confocal images of fluo-4 fluorescence were acquired at 19 - 42 Hz using a Zeiss plan-Apochromat 40× 1.3 N.A. oil-immersion objective. Fluo-4 and fluo-3FF fluorescence was excited by the 488 nm line of a 200 mW argon ion laser (Laser-Fertigung, Hamburg, Germany) and was captured at wavelengths above 505 nm. The pinhole was set to provide a confocal optical slice below 1.2 μm.

To avoid any bleed-through in immunofluorescence experiments, SMCs were double labelled using fluorophores with extremely well separated emission spectra: Alexa Fluor 488 (Em = 519 nm) and Alexa Fluor 633 (Em = 647 nm). Dual excitation, using the multitrack mode of an LSM 510, was performed by the 488 nm line of a 200 mW argon ion laser and the 633 nm line of a 15 mW helium/neon ion laser, respectively. The emitted fluorescence signal was filtered using 505 nm - 550 nm bandpass filter (for the green IP<sub>3</sub>R label) and 650 nm longpass filter (for the red RyR label). The adequacy of the imaging protocol applied to the double-labelled SMCs was confirmed by control experiments on the single-labelled cells.

## 2.7. Electrical recordings

The cell membrane potential was monitored using perforated-patch (200 μg/ml amphotericin B) tight seal recording in the current-clamp mode of an Axopatch 200A (Molecular Devices Co., CA, USA) patch-clamp amplifier. This allowed low resistance access to the cell while minimally interfering with [Ca<sup>2+</sup>]<sub>i</sub>. The cell was bathed in PSS and dialysed with solution composed of (mM): KCl 120, KH<sub>2</sub>PO<sub>4</sub> 5, MgSO<sub>4</sub> 5, Na<sub>2</sub>ATP 5, Li<sub>2</sub>GTP, Hepes 10; pH was adjusted to 7.4 with KOH. Recording of the cell membrane potential was synchronised with confocal imaging using a TTL synchronising pulse generated by the confocal scanner at the beginning of the time series protocol.

Membrane currents were recorded using the conventional whole-cell patch clamp technique using an Axopatch 200A or a Multiclamp 700A patch-clamp amplifier (Molecular Devices Co., CA, USA). Liquid junction potential was nulled with the offset circuit of the amplifier before seal formation. Pipette and cell capacitance and series resistance were compensated electronically using corresponding amplifier controls. No electronic compensation for the leakage conductance was introduced. The electrical signals were filtered at 1 kHz (-3 dB frequency) by a four-pole low-pass Bessel filter. Voltage protocols were generated and electrical signals were digitised at 5 kHz using a DigiData 1200 or a Digidata 1322A hosted by a Pentium PC running either pCLAMP 6.0 or pClamp 8.2 software (Molecular Devices Co., CA, USA).

Muscarinic cationic current ( $mI_{cat}$ ) activated by external application of 10  $\mu$ M CCh (see above) was recorded at holding potential of  $-50$  mV. Background holding current was measured before CCh application. In these experiments, the composition of extracellular solution was (mM): CsCl 120, CaCl<sub>2</sub> 2.5, MgCl<sub>2</sub> 1.2, glucose 12, Hepes 10 (pH 7.4 adjusted with CsOH) and the composition of the pipette solution was (in mM): CsCl 80, MgATP 1, creatine 5, glucose 5, Hepes 10 (pH adjusted to 7.4 with CsOH). To unmask any direct effect of the IP<sub>3</sub>R inhibitor 2-APB on  $mI_{cat}$ , the effect of 2-APB on  $mI_{cat}$  mediated via inhibition of IP<sub>3</sub>R-mediated Ca<sup>2+</sup> release was eliminated by clamping  $[Ca^{2+}]_i$  at 100 nM with 4.6 mM CaCl<sub>2</sub> / 10 mM BAPTA buffer added to the pipette solution [24].

Voltage-gated Ca<sup>2+</sup> currents were evoked by 500-ms voltage steps to 0 mV applied from a holding potential of  $-80$  mV every 30 s. In these experiments, the composition of the extracellular solution was (mM): NaCl 135, CsCl 6, CaCl<sub>2</sub> 2.5, MgCl<sub>2</sub> 1.2, glucose 12, Hepes 10 (pH 7.4 adjusted with NaOH) and the composition of the pipette solution was (in mM): CsCl 126, MgSO<sub>4</sub> 5, Na<sub>2</sub>ATP 5, Li<sub>2</sub>GTP 1 (pH adjusted to 7.4 with CsOH and  $[Ca^{2+}]_i$  was clamped at 20 nM with 2.6 mM CaCl<sub>2</sub> / 10 mM EGTA buffer).

## 2.8. Reagents

Protease (Type X), collagenase (type 1A), soybean trypsin inhibitor (Type II-S), bovine serum albumin, adenosine 5' triphosphate (ATP, magnesium salt), guanosine 5' triphosphate (GTP, disodium salt), creatine, N-2-hydroxyethylpiperazine-N'-2-ethanesulphonic acid (HEPES), 1,2-bis(2-aminophenoxy)-ethane-N,N,N',N'-tetraacetic acid (BAPTA), ethylene glycol-bis(2-aminoethylether)-N,N,N',N'-tetraacetic acid (EGTA), carbamylcholine chloride (carbachol), 1,3,7-trimethylxanthine (caffeine), dimethyl sulfoxide (DMSO), paraformaldehyde and Triton X-100 were obtained from Sigma Chemical Co., Poole, Dorset, UK. Fluo-4 acetoxymethyl ester, Alexa Fluor 488 conjugated chicken anti-rabbit IgG (H+L), Alexa Fluor 633 conjugated goat anti-mouse IgG (H+L) and pluronic F-127 were obtained from Invitrogen Ltd., Paisley, UK. Fluo-3FF acetoxymethyl ester was from TefLabs, Austin, Texas, USA. All other chemicals were from BDH Laboratory Supplies (AnalaR grade), Pool, UK.

## 2.9. Data analysis

Image processing was carried out using an Indy workstation (Silicon Graphic, Inc., Mountain View, CA, USA) with custom routines written in IDL (Research Systems, Inc., Boulder, CO, USA). The final figures were produced using MicroCal Origin (MicroCal Software Inc., Northampton, MA, USA) and CorelDraw 7.0 (Corel Corporation, Canada). Where appropriate, data are expressed as mean values  $\pm$  SEM for the number of cells ( $n$ ) analysed. Comparative analysis of the data groups was performed using Student's *t*-test for paired or unpaired samples, as appropriate, with the threshold for statistical significance set at the 0.05 level.

## 3. Results

### 3.1. Action potential discharge following muscarinic receptor activation is coupled to a sub-PM $[Ca^{2+}]_i$ upstroke (SPCU)

The dynamics of the change in intracellular Ca<sup>2+</sup> concentration ( $[Ca^{2+}]_i$ ) following muscarinic receptor activation were related to the changes in the cell membrane potential ( $V_m$ ). SMCs freshly isolated from the guinea-pig ileum were preloaded with the high affinity Ca<sup>2+</sup> indicator fluo-4 and bathed in PSS (see Methods). High speed *x-y* confocal Ca<sup>2+</sup> imaging (acquisition rate varied between 19 and 42 Hz) was combined with recording of  $V_m$  in perforated-patch configuration to minimally perturb endogenous  $[Ca^{2+}]_i$  ( $n = 4$ ). Muscarinic receptors were stimulated by brief applications of 10  $\mu$ M carbachol (CCh)



through a glass micropipette positioned within 100 – 200  $\mu\text{m}$  of the cell surface. This revealed that the discharge of each action potential (AP) following muscarinic receptor activation was associated with a  $[\text{Ca}^{2+}]_i$  transient which was initiated by an abrupt increase of  $[\text{Ca}^{2+}]_i$  at multiple subplasmalemmal (sub-PM) regions. The dynamics of  $[\text{Ca}^{2+}]_i$  changes in these sub-PM regions of initiation was therefore analysed. In the example shown in Fig. 1, the first 60-ms application of 10  $\mu\text{M}$  CCh triggered three APs but no sustained membrane depolarization (probably because equilibrium CCh concentration near the cell membrane was not achieved). Even though after each action potential the cell membrane was repolarized to a resting level (black trace, Fig. 1A and B), each AP was associated with a stepwise increase of the global  $[\text{Ca}^{2+}]_i$  (green trace Fig. 1A and B). The second 600-ms application of 10  $\mu\text{M}$  CCh caused membrane depolarization, which was associated with increased frequency of APs. Within 1.5 second depolarization became so extreme that AP discharge ceased (black trace, Fig. 1A and C). The global  $[\text{Ca}^{2+}]_i$  response caused by the 600-ms CCh application (green trace Fig. 1A and C) consisted of an initial large-amplitude transient followed by a sustained phase showing small amplitude oscillations. In both cases, however, each AP was coupled to a very brief abrupt  $[\text{Ca}^{2+}]_i$  transient (red trace, Fig. 1) at multiple sub-PM regions (illustrated by (ii) and outlined in (i), Fig. 1A). The spatio-temporal profiles of intracellular  $\text{Ca}^{2+}$  mobilisations associated with the first AP following the first CCh application, and with the two APs following the second CCh application, are illustrated by two galleries of 18 sequential confocal images (Fig. 1 B and C, respectively). Comparing the images in the galleries revealed a remarkable constancy of the positions of the sites of initiation of  $\text{Ca}^{2+}$  mobilisation associated with each AP. The lack of spatial uniformity suggests that rather than  $\text{Ca}^{2+}$  entry through voltage-gated  $\text{Ca}^{2+}$  channels (VGCCs) these signals reflect  $\text{Ca}^{2+}$  release from non-uniformly distributed sub-PM  $\text{Ca}^{2+}$  stores. Because of their location and robust onset kinetics, we refer to these events hereafter as the “sub-PM  $[\text{Ca}^{2+}]_i$  upstroke (SPCU)”.

Spatio-temporal patterns of CCh-induced  $[\text{Ca}^{2+}]_i$  mobilisation in non-patched SMCs are illustrated by Fig. 2 showing the results obtained in 5 different cells. Muscarinic receptors were activated by 10  $\mu\text{M}$  CCh either superfused through the experimental bath (Fig. 2A) or applied to the cell as a 600-ms pulse through a glass micropipette (Fig. 2B-E). In all plots, the green traces show the temporal profile of the global  $[\text{Ca}^{2+}]_i$  changes, while red traces show the dynamics of  $[\text{Ca}^{2+}]_i$  changes averaged at multiple sub-PM regions (outlined in the images; insets on the plots) where CCh-induced  $[\text{Ca}^{2+}]_i$  transients were initiated. The galleries show sequential confocal images of fluo-4 fluorescence acquired during the periods marked by a grey background in the plots, respectively. In all cases CCh-induced  $[\text{Ca}^{2+}]_i$  transients were initiated by a SPCU (depicted by the arrowheads on the galleries). Muscarinic receptor activation evoked a SPCU independently of the extent of myocyte contraction ( $n = 147$ ), suggesting that this phenomenon is not a result of the increase in the local density of  $\text{Ca}^{2+}$ -release units, which could be caused by change in SMC geometry. In the vast majority of cases (97%) two phases can be clearly distinguished in the  $\text{Ca}^{2+}$  responses to CCh: (1) an initial high-amplitude  $[\text{Ca}^{2+}]_i$  transient and (2) a delayed increase of global  $[\text{Ca}^{2+}]_i$  characterised by a smaller amplitude and a tendency to oscillation.

### 3.2. Genesis of SPCU depends on both voltage-gated $\text{Ca}^{2+}$ entry and $\text{Ca}^{2+}$ release from the SR

Muscarinic cationic channels in gastro-intestinal smooth muscles have very low, if any, permeability for  $\text{Ca}^{2+}$  [25-27], and the major physiological role of muscarinic cationic current ( $\text{mI}_{\text{cat}}$ ) is to depolarise the cell membrane and to trigger the opening of voltage-gated  $\text{Ca}^{2+}$  channels (VGCCs), pharmacological blockade of which virtually completely abolishes muscarinic contractile responses [28, 29]. We therefore tested the effect of VGCC block on CCh-induced  $[\text{Ca}^{2+}]_i$  mobilisation. In this and all subsequent experiments we analysed the

dynamics of  $[Ca^{2+}]_i$  changes at multiple sub-PM regions of initiation of CCh-induced  $[Ca^{2+}]_i$  mobilisation. In control, the response to CCh was initiated by a SPCU (Fig. 3A, red trace) and then rapidly propagated through the entire cell volume (Fig. 3A, gallery a). The initial  $[Ca^{2+}]_i$  transient was followed by a lower-amplitude sustained phase with two  $[Ca^{2+}]_i$  oscillations (Fig. 3A, red trace). Block of voltage-gated  $Ca^{2+}$  channels with 5  $\mu$ M nicardipine (30-s incubation) eliminated the SPCU (Fig. 3A, gallery b) and substantially attenuated, but did not abolish, both the initial and delayed phase of the CCh-induced  $[Ca^{2+}]_i$  transient (Fig. 3A, green trace). In the presence of nicardipine, the peak of CCh-induced  $[Ca^{2+}]_i$  transient (green trace) was reduced by 60%, time-to-peak was increased from 0.8 s to 1.3 s and the  $Ca^{2+}$  wave propagated more slowly than in control (Fig. 3A, gallery b). These results suggest that: (1) the SPCU requires voltage-gated  $Ca^{2+}$  entry and (2)  $Ca^{2+}$  entry through VGCCs is not the only source of  $Ca^{2+}$  upon muscarinic  $[Ca^{2+}]_i$  mobilisation.

To evaluate the contribution of  $Ca^{2+}$  release from intracellular stores to CCh-induced  $[Ca^{2+}]_i$  mobilisation, the effect of  $Ca^{2+}$  store depletion was tested. In control, CCh induced a rapidly propagating  $[Ca^{2+}]_i$  wave (Fig. 3B, gallery a) which was initiated by a SPCU (regions of initiation are outlined in the image, Fig. 3B). The initial  $[Ca^{2+}]_i$  transient was followed by a lower-amplitude sustained phase showing multiple small-amplitude but high-frequency oscillations (Fig. 3B, red trace). A 10-min incubation of the ileal SMCs with 10  $\mu$ M cyclopiazonic acid (CPA), a reversible inhibitor of the sarco/endoplasmic reticulum  $Ca^{2+}$ -ATPase (SERCA), resulted in complete depletion of the intracellular  $Ca^{2+}$  stores in this cell type, as we have previously demonstrated using flash release of "caged"  $IP_3$  preloaded into the cells through the patch pipette [24]. Depletion of  $Ca^{2+}$  stores with CPA treatment eliminated the SPCU, reduced the peak amplitude of the initial CCh-induced  $[Ca^{2+}]_i$  transient by 80 %, increased time-to-peak from 0.7 s to 1.4 s and virtually completely abolished the delayed phase of the response (Fig. 3B, green trace). With  $Ca^{2+}$  stores depleted, the residual  $[Ca^{2+}]_i$  response was spatially uniform (Fig. 3B, gallery b), consistent with  $Ca^{2+}$  entry through VGCCs. This was further confirmed when subsequent block of VGCCs with 5  $\mu$ M nicardipine (while keeping  $Ca^{2+}$  stores depleted) completely abolished  $[Ca^{2+}]_i$  mobilisation in response to CCh (Fig. 3B, magenta trace and gallery c). This also directly demonstrates that muscarinic cationic channels in SMCs of the guinea-pig ileum are virtually impermeable to  $Ca^{2+}$ .

Summing up, the above results show that both  $Ca^{2+}$  entry through VGCCs and  $Ca^{2+}$  release from intracellular  $Ca^{2+}$  stores contribute to the SPCU and full scale  $[Ca^{2+}]_i$  mobilisation in response to muscarinic stimulation.

### 3.3. SPCU results from $IP_3R$ - mediated $Ca^{2+}$ release facilitated by $Ca^{2+}$ entry through VGCCs

To examine what type of the SR  $Ca^{2+}$  release channels is involved in SPCU and what the mechanisms underlie the subsequent transient and delayed phases of CCh-induced  $[Ca^{2+}]_i$  mobilisation, we studied the effects of successive cumulative inhibitions of RyRs,  $IP_3$ Rs and VGCCs on  $Ca^{2+}$  responses to CCh. The SMCs were incubated for 10 min with 50 – 100  $\mu$ M tetracaine [30-32] to block RyRs and with 2  $\mu$ M xestospongin C [16, 33, 34] to block  $IP_3$ Rs. In the example shown in Fig. 4, control response to CCh consisted of a  $[Ca^{2+}]_i$  transient initiated by a SPCU and followed by numerous  $[Ca^{2+}]_i$  oscillations of gradually decreasing amplitude (Fig.4, red trace and gallery a). Nevertheless, block of RyRs by tetracaine did not abolish the SPCU and even slightly (5 %) augmented the initial  $[Ca^{2+}]_i$  transient, but abolished the delayed phase of the response to CCh and the  $[Ca^{2+}]_i$  oscillations (Fig.4, green trace and gallery b). The slight increase of the initial  $[Ca^{2+}]_i$  transient may result from the increase in the SR  $Ca^{2+}$  load following tetracaine treatment [31]. The overall effect of

tetracaine on CCh-induced  $[Ca^{2+}]_i$  mobilisation implies that RyRs play little role, if any, in the SPCU, but are important for the sustained response to CCh and in  $[Ca^{2+}]_i$  oscillations.

A subsequent incubation of the myocyte with 2  $\mu$ M xestospongine C (in the presence of tetracaine) abolished the SPCU, inhibited the initial  $[Ca^{2+}]_i$  transient by 95 % and increased the time-to-peak from 1 s to 2.5 s (Fig.4, magenta trace c). The remaining CCh-induced  $[Ca^{2+}]_i$  transient was characterised by a slow and spatially uniform rising phase, consistent with  $Ca^{2+}$  entry through VGCCs (Fig.4, gallery c). This observation indicates that the SPCU strongly depends on the ability of IP<sub>3</sub>R to release  $Ca^{2+}$ .

Subsequent block of VGCCs with 5  $\mu$ M nifedipine (1-min incubation) completely abolished the residual response to CCh (Fig. 4, black trace and gallery d), thus confirming the idea that the uniform transient increase of  $[Ca^{2+}]_i$  triggered by CCh in the presence of tetracaine and xestospongine C was caused by  $Ca^{2+}$  entry through VGCCs.

It is known, however, that commercially available inhibitors of IP<sub>3</sub>R-mediated  $Ca^{2+}$ -release, namely xestospongine C and 2-aminoethoxy-diphenylborate (2-APB), may affect some other mechanisms of intracellular  $Ca^{2+}$  homeostasis. Since the key event in muscarinic  $[Ca^{2+}]_i$  mobilisation seems to be the  $Ca^{2+}$  entry through VGCCs, we tested the effect of 2  $\mu$ M xestospongine C and 30  $\mu$ M 2-APB on the voltage-gated  $Ca^{2+}$  current ( $I_{Ca}$ ) evoked by a 500-ms voltage steps from -80 to +0 mV under whole-cell voltage clamp conditions (Fig. 5). The currents were recorded in  $Cs^+/Na^+$ -containing solutions (see Methods) while the pipette solution was supplemented with 5 mM ATP and 1 mM GTP to minimise rundown of  $I_{Ca}$ . The peak amplitude of  $I_{Ca}$  (Fig. 5A) evoked by repetitive (applied at 30-s intervals) voltage steps was normalised to the peak amplitude of  $I_{Ca}$  evoked by the first voltage step ( $I_{test}/I_{first}$ ) and plotted over time (Fig. 5B) in control ( $n = 7$ ) and following application of 2  $\mu$ M xestospongine C ( $n = 4$ ) or 30  $\mu$ M 2-APB ( $n = 5$ ). This revealed that after allowing for  $I_{Ca}$  rundown, the reduction of the current amplitude was by a further 74% during 10 min (from  $I_{test}/I_{first} = 0.779 \pm 0.058$  in control to  $I_{test}/I_{first} = 0.184 \pm 0.013$  in xestospongine C; significant difference:  $p = 0.00018$ ) can account for the inhibitory effect of xestospongine C on VGCCs. In contrast, 2-APB during the same period augmented  $I_{Ca}$  (taking into account the  $I_{Ca}$  rundown) on average by 35% (from  $I_{test}/I_{first} = 0.779 \pm 0.058$  in control to  $I_{test}/I_{first} = 1.056 \pm 0.159$  in 2-APB; not significantly different:  $p = 0.073$ ). Thus, the inhibitory effect of 2  $\mu$ M xestospongine C on CCh-induced  $[Ca^{2+}]_i$  mobilisation may partially (since CCh-induced  $[Ca^{2+}]_i$  transient was not abolished by xestospongine C but was eliminated by subsequent block of VGCCs with nifedipine; Figs. 4) result from inhibition of VGCCs by this compound.

Taking into account that activation of VGCCs in response to muscarinic receptor activation is caused by depolarisation evoked by  $mI_{cat}$ , and thus will not occur if the muscarinic cationic channels are blocked, the effects of 30  $\mu$ M 2-APB on  $mI_{cat}$  (Fig 6A) were tested. The current induced by 10  $\mu$ M CCh was recorded under whole-cell voltage clamp at holding potential of -50 mV using  $Cs^+$ -containing pipette and bathing solutions (see Methods). Since  $mI_{cat}$  is  $Ca^{2+}$ -sensitive [24, 26, 35-37], to eliminate the effect of 2-APB caused by inhibition of IP<sub>3</sub>R-mediated  $Ca^{2+}$  release,  $[Ca^{2+}]_i$  was clamped at 100 nM (see Methods). Each SMC was stimulated twice with a 10-min interval between subsequent CCh applications. The response to the second CCh application (Test) was related to the response to the first CCh application (Control). In control external solution, the peak amplitude of the test  $mI_{cat}$  (Fig. 6Aa) constituted on average  $78 \pm 4$  % ( $n = 6$ ) of the control  $mI_{cat}$  (Fig. 6Ac). Incubation with 30  $\mu$ M 2-APB for 8 min prior to the second CCh application reduced the peak amplitude of the test  $mI_{cat}$  (Fig. 6Ab) to the  $30 \pm 2$  % ( $n = 6$ ) of the control  $mI_{cat}$  (Fig. 6Ac). Thus, 30  $\mu$ M 2-APB caused inhibition of  $mI_{cat}$  by 61.5 % (significant difference:  $p = 0.00019$ ).



However, in terms of CCh-induced  $[Ca^{2+}]_i$  mobilisation, the amplitude of  $mI_{cat}$  is not of as much importance (since this current is not conducted by  $Ca^{2+}$  under quasi-physiological conditions, see above) as the level of the cell membrane depolarization caused by this current. Indeed, any ionic current cannot change the cell membrane potential ( $V_m$ ) beyond the level of the reversal potential of the current. In the case when the input resistance of the cell is relatively high (such as at resting condition) even a small amplitude current can produce a substantial shift in  $V_m$ . We therefore tested the effect of 30  $\mu$ M 2-APB on CCh-induced membrane depolarization (Fig. 6B). The SMCs were bathed in PSS and dialysed with  $K^+$ / $Na^+$ -containing solution (see Methods). Application of 10  $\mu$ M CCh shifted  $V_m$  from  $-33 \pm 2$  mV to  $-4 \pm 1$  mV ( $n = 5$ ) in control (Ba) and from  $-29 \pm 4$  mV to  $-5 \pm 1$  mV ( $n = 5$ ) in 30  $\mu$ M 2-APB (Bb), ( $n = 5$ ). The values of the magnitude ( $\Delta V_m$ ) of membrane depolarization (Bc) caused by CCh in control ( $29 \pm 2$  mV) and in 2-APB ( $24 \pm 4$  mV), as well as extent of the CCh-induced depolarization in control and in 2-APB were not significantly different ( $p = 0.23$  and  $p = 0.52$ , respectively). This validates 2-APB as pharmacological tool for study of the role of  $IP_3Rs$  in CCh-induced  $[Ca^{2+}]_i$  mobilisation.

Inhibition of  $IP_3Rs$  by 10-min incubation of the SMC with 30  $\mu$ M of 2-APB abolished the SPCU, inhibited the CCh-induced  $[Ca^{2+}]_i$  transient by 79% and increased time-to-peak from 0.5 s to 4.5 s (Fig. 7C, green trace). Subsequent block of VGCCs with 5  $\mu$ M nicardipine (30-s incubation) completely abolished the residual response to CCh (Fig. 6C, magenta trace and gallery c). This observation confirmed our conclusion that following muscarinic receptor activation  $Ca^{2+}$  entry through VGCCs facilitates the initial  $IP_3R$ -mediated  $Ca^{2+}$  release at sub-PM regions leading to a SPCU, which in turn engages full scale  $[Ca^{2+}]_i$  mobilisation.

The effects of the  $Ca^{2+}$  store depletion, inhibition of VGCCs, RyRs and  $IP_3Rs$  on the CCh-induced  $[Ca^{2+}]_i$  transient initiated by SPCU are summarised in Fig. 7. In all experiments the fluo-4 loaded SMCs were stimulated with 600-ms pulses of 10  $\mu$ M CCh, which were applied to the same cell at least twice with a 10-min interval between subsequent CCh applications (Fig. 7A). The increase in the normalised intensity of fluo-4 fluorescence ( $\Delta F/F_0$ ) averaged at multiple sub-PM regions of initiation of the CCh-induced  $[Ca^{2+}]_i$  transient was then plotted over time. The response to the succeeding CCh application (Test) was related to the response to the first CCh application (Control). The test response was obtained either in the control external solution (to evaluate reproducibility of CCh-induced  $[Ca^{2+}]_i$  transients) or following a 10-min incubation of the SMC with a drug or combination of several drugs. When the effect of VGCC block on muscarinic  $[Ca^{2+}]_i$  mobilisation was tested, nicardipine was applied 30 s – 1 min before pulse of CCh to minimise possible effect of VGCC block on the SR  $Ca^{2+}$  load. Two parameters were examined and are summarised in the bar diagram plots: (1) relative change in peak amplitude,  $(\Delta F/F_0)_{Test}/(\Delta F/F_0)_{Control}$  (Fig. 7B) and (2) relative change in time-to-peak,  $(t_{peak})_{Test}/(t_{peak})_{Control}$  (Fig. 7C). This revealed that: (i) in control external solution, the peak amplitude of the test response (Fig. 7Aa) constituted on average  $92 \pm 5\%$  ( $n = 29$ ) of the control response (Fig. 7B), while time-to-peak was on average  $102 \pm 5\%$  of that in control response (Fig. 7C); (ii) block of RyRs with either 100  $\mu$ M ryanodine ( $(\Delta F/F_0)_{Test}/(\Delta F/F_0)_{Control} = 84 \pm 10\%$ ,  $(t_{peak})_{Test}/(t_{peak})_{Control} = 116 \pm 15\%$ ,  $n = 7$ ) or with 50 – 100  $\mu$ M tetracaine ( $(\Delta F/F_0)_{Test}/(\Delta F/F_0)_{Control} = 85 \pm 6\%$ ,  $(t_{peak})_{Test}/(t_{peak})_{Control} = 108 \pm 5\%$ ,  $n = 14$ ) had no significant effect on either amplitude ( $p = 0.47$  and  $p = 0.37$ , respectively) or kinetics ( $p = 0.25$  and  $p = 0.44$ , respectively) of the initial  $[Ca^{2+}]_i$  transient; (iii) depletion of intracellular  $Ca^{2+}$  stores with 10  $\mu$ M CPA ( $(\Delta F/F_0)_{Test}/(\Delta F/F_0)_{Control} = 11.5 \pm 6\%$ ,  $(t_{peak})_{Test}/(t_{peak})_{Control} = 284 \pm 18\%$ ,  $n = 6$ ) reduced the peak amplitude by 87.5% ( $p = 1.3 \times 10^{-7}$ ) and increased time-to-peak by 178% ( $p = 1.7 \times 10^{-15}$ ); (iv) block of VGCCs with 5  $\mu$ M nicardipine ( $(\Delta F/F_0)_{Test}/(\Delta F/F_0)_{Control} = 9 \pm 1\%$ ,  $(t_{peak})_{Test}/(t_{peak})_{Control} = 334 \pm 27\%$ ,  $n = 18$ ) reduced the peak amplitude by 90% ( $p = 5.7 \times 10^{-18}$ ) and increased time-to-peak by 227% ( $p = 5.2 \times 10^{-14}$ ); (v) simultaneous block of VGCCs and RyRs with 5  $\mu$ M nicardipine / 50 – 100  $\mu$ M

tetracaine ( $(\Delta F/F_0)_{\text{Test}}/(\Delta F/F_0)_{\text{Control}} = 9 \pm 3\%$ ,  $(t_{\text{peak}})_{\text{Test}}/(t_{\text{peak}})_{\text{Control}} = 360 \pm 60\%$ ,  $n = 6$ ) reduced the peak amplitude by 90 % ( $p = 2.2 \times 10^{-9}$ ) and increased time-to-peak by 253 % ( $p = 8.7 \times 10^{-11}$ ); (vi) block of IP<sub>3</sub>Rs with 2  $\mu\text{M}$  xestospongine C ( $(\Delta F/F_0)_{\text{Test}}/(\Delta F/F_0)_{\text{Control}} = 22 \pm 6\%$ ,  $(t_{\text{peak}})_{\text{Test}}/(t_{\text{peak}})_{\text{Control}} = 261 \pm 26\%$ ,  $n = 15$ ) reduced the peak amplitude by 76 % ( $p = 1.2 \times 10^{-11}$ ) and increased time-to-peak by 159 % ( $p = 3.3 \times 10^{-10}$ ); block of IP<sub>3</sub>Rs with 30  $\mu\text{M}$  2-APB ( $(\Delta F/F_0)_{\text{Test}}/(\Delta F/F_0)_{\text{Control}} = 23 \pm 3\%$ ,  $(t_{\text{peak}})_{\text{Test}}/(t_{\text{peak}})_{\text{Control}} = 283 \pm 22\%$ ,  $n = 16$ ) reduced the peak amplitude by 75 % ( $p = 2.0 \times 10^{-13}$ ) and increased time-to-peak by 177 % ( $p = 3.6 \times 10^{-13}$ ); (vii) simultaneous block of RyRs and IP<sub>3</sub>Rs with 50 – 100  $\mu\text{M}$  tetracaine / 2  $\mu\text{M}$  xestospongine C ( $(\Delta F/F_0)_{\text{Test}}/(\Delta F/F_0)_{\text{Control}} = 10 \pm 4\%$ ,  $(t_{\text{peak}})_{\text{Test}}/(t_{\text{peak}})_{\text{Control}} = 287 \pm 16\%$ ,  $n = 6$ ) reduced the peak amplitude by 89 % ( $p = 3.4 \times 10^{-9}$ ) and increased time-to-peak by 181 % ( $p = 2.1 \times 10^{-16}$ ); (viii) simultaneous block of RyRs and IP<sub>3</sub>Rs with 50 – 100  $\mu\text{M}$  tetracaine / 30  $\mu\text{M}$  2-APB ( $(\Delta F/F_0)_{\text{Test}}/(\Delta F/F_0)_{\text{Control}} = 9 \pm 2\%$ ,  $(t_{\text{peak}})_{\text{Test}}/(t_{\text{peak}})_{\text{Control}} = 291 \pm 46\%$ ,  $n = 6$ ) reduced the peak amplitude by 90 % ( $p = 2.1 \times 10^{-8}$ ) and increased time-to-peak by 185 % ( $p = 2.1 \times 10^{-10}$ ); (ix) block of VGCCs (with 5  $\mu\text{M}$  nifedipine) following intracellular Ca<sup>2+</sup> store depletion (with 10  $\mu\text{M}$  CPA), or simultaneous block of VGCCs and IP<sub>3</sub>Rs (with either 5  $\mu\text{M}$  nifedipine / 2  $\mu\text{M}$  xestospongine C or 5  $\mu\text{M}$  nifedipine / 30  $\mu\text{M}$  2-APB) completely abolished [Ca<sup>2+</sup>]<sub>i</sub> mobilisation in response to CCh. Thus, significant inhibition of the CCh-induced [Ca<sup>2+</sup>]<sub>i</sub> transient was associated with significant reduction in its rate of rise, which is indicative of the elimination of the SPCU. Altogether these results strongly suggest that following muscarinic stimulation, SPCU results from Ca<sup>2+</sup> release mediated via IP<sub>3</sub>Rs, which are activated synergistically by (1) IP<sub>3</sub> mobilised via the M<sub>3</sub> – G<sub>q/11</sub> – PLC $\beta$  pathway, and (2) Ca<sup>2+</sup> entering the cell through VGCCs activated via the M<sub>2</sub> – G<sub>o</sub> – mI<sub>cat</sub> – membrane depolarization pathway.

### 3.4. Sub-plasmalemmal SR elements are enriched with IP<sub>3</sub>Rs

The above hypothesis suggests: (1) a sub-PM location of the SR elements in ileal SMCs and (2) the expression of IP<sub>3</sub>Rs in these SR elements.

Intracellular Ca<sup>2+</sup> stores visualised with the low-affinity ( $k_{d(\text{Ca})} = 42 \mu\text{M}$ ) Ca<sup>2+</sup> indicator fluo-3FF (Fig. 8A) consisted of a sub-PM SR network and some central elements ( $n = 47$ ). This spatial organisation of intracellular Ca<sup>2+</sup> stores is generally similar to that we have previously demonstrated in the rabbit portal vein myocytes using DiOC<sub>6</sub> and BODIPY TR-X ryanodine [38] and SMCs of the guinea-pig mesenteric artery using brefeldin A BODIPY 558/568 (unpublished observation).

Immunodetection of IP<sub>3</sub>Rs (with antibody specific for type 1 IP<sub>3</sub>R) and RyRs (with antibody targeting type 1, type 2 and type 3 RyRs) by double labelling ( $n = 18$ ) of the same SMC (see Methods) revealed that type 1 IP<sub>3</sub>Rs are predominantly expressed in sub-PM SR elements over the entire periphery of the cell, while RyRs are absent from the ends of the SMC, but are seen in some central sub-PM and deep SR elements (Fig. 8B). Based on the results of the cell fractionation and binding studies of the longitudinal muscle layer of the guinea-pig ileum, showing that the overall stoichiometric ratio of RyRs to IP<sub>3</sub>Rs in SMCs from this tissue is 1:9-10, the existence of a Ca<sup>2+</sup>-storage compartment devoid of RyRs but equipped with IP<sub>3</sub>Rs has been suggested previously [39]. This is in agreement with our finding showing that only a few elements of the SR in the central region of the SMC represent a Ca<sup>2+</sup> store where the type 1 IP<sub>3</sub>Rs and RyRs are co-expressed (yellowish spots; Fig. 8B).

Close proximity of the IP<sub>3</sub>R-enriched SR elements to the cell plasma membrane facilitates an abrupt IP<sub>3</sub>R-mediated Ca<sup>2+</sup>-release when [Ca<sup>2+</sup>]<sub>i</sub> and [IP<sub>3</sub>]<sub>i</sub> rapidly rise in the restricted microvolume between the SR and plasmalemma, as observed in the case of activation of muscarinic receptors with CCh (Fig. 8C). In contrast, when the same cell was stimulated with 5 mM caffeine, which activates RyRs to release Ca<sup>2+</sup>, the Ca<sup>2+</sup> wave developed

initially in the cell centre (where RyRs are predominant) and only then spreads to the cell periphery (Fig. 8C). The difference in the dynamics of  $[Ca^{2+}]_i$  mobilisation at three regions within the SMC following stimulation with CCh and caffeine is emphasised by the plots showing the time course of the fluo-4 fluorescence averaged within each of the three regions (Fig. 8D). In response to CCh  $[Ca^{2+}]_i$  rapidly increased at all three regions: IP<sub>3</sub>R-mediated  $Ca^{2+}$  release leading to a SPCU. In contrast, in response to caffeine, RyRs released  $Ca^{2+}$  initially within the region 1, then  $Ca^{2+}$  wave reached the region 2 and only then, with a more substantial delay, it arrived at region 3.

### 3.5. IP<sub>3</sub>R-mediated $Ca^{2+}$ release is essential for force generation

Several lines of evidence presented above strongly suggest that in SMCs freshly isolated from the guinea-pig ileum,  $[Ca^{2+}]_i$  mobilisation in response to muscarinic receptor activation is initiated by a SPCU resulting from an abrupt IP<sub>3</sub>R-mediated  $Ca^{2+}$  release at multiple sub-PM regions where it is facilitated by  $Ca^{2+}$  entry through VGCCs. Under conditions when the SPCU is abolished (by inhibition of IP<sub>3</sub>Rs or VGCCs), the global  $[Ca^{2+}]_i$  mobilisation within the SMC is substantially attenuated (Fig. 7). It therefore seems likely that this IP<sub>3</sub>R-mediated  $Ca^{2+}$  release is a key element in the chain of events resulting in the muscarinic contractile response. To test this we examined the effect of inhibition of IP<sub>3</sub>Rs and RyRs on isometric force generated in response to muscarinic stimulation of a smooth muscle strip freshly dissected from the longitudinal layer of the guinea-pig ileum (Fig. 9). The strips were stimulated with 2  $\mu$ M CCh, which was transiently applied to the same strip at least twice. The response to the second CCh application was referred to as the test response, while the response to the first CCh application was referred to as the control response. The test response was obtained either in the control external solution to evaluate reproducibility of the responses to CCh (Fig. 9A), or following a 7-min incubation of the strip with either 30  $\mu$ M 2-APB (Fig. 9B) or 100  $\mu$ M tetracaine (Fig. 9C). The maximal isometric force ( $F_o$ ) detected during the test response was then normalised to that during the control response and compared in control and following incubation with the drugs (Fig. 9D). This revealed that: (i) in control external solution, the peak amplitude of the test response constituted on average  $98 \pm 7\%$  ( $n = 8$ ) of the control response; (ii) inhibition of IP<sub>3</sub>Rs with 30  $\mu$ M 2-APB ( $(F_o)_{Test}/(F_o)_{Control} = 26.5 \pm 5\%$ ,  $n = 4$ ) reduced the peak isometric force by 73% ( $p = 0.0006$ ); (iii) inhibition of RyRs with 100  $\mu$ M tetracaine ( $(F_o)_{Test}/(F_o)_{Control} = 29 \pm 10\%$ ,  $n = 3$ ) reduced the peak isometric force by 70% ( $p = 0.001$ ). This demonstrates that both IP<sub>3</sub>R- and RyR-mediated  $Ca^{2+}$  release are required for full scale contractile response to 2  $\mu$ M CCh. However, in contrast to tetracaine, 2-APB also abolished spontaneous oscillations of isometric tension observed in control (compare Fig. 9B and 9C).

On the other hand, a SPCU should activate large conductance  $Ca^{2+}$ -activated  $K^+$  channels (BK channels) in the cell membrane, which may lead to membrane hyperpolarization and, as a result, to a decrease of  $Ca^{2+}$  entry through VGCCs [11], thus slowing down  $[Ca^{2+}]_i$  mobilization and perhaps the contractile response. This, however, was not observed. Indeed, even though the peak of the CCh-induced  $[Ca^{2+}]_i$  transient was associated with some minor (about 8 mV) transient repolarization of the cell membrane (Fig. 1C), inhibition of IP<sub>3</sub>Rs with 2-APB did not accelerate the contractile response to CCh, and its kinetics remained the same in control and following 2-APB or tetracaine pre-treatment (see insets in Fig. 9A-C). Nevertheless, we tested the effect of a selective inhibitor of BK channels, paxilline [40] on CCh-induced isometric force using a similar experimental protocol (Fig. 10). Exposure of the muscle strips to 0.1  $\mu$ M paxilline did not change the tonic tension, but augmented the amplitude of spontaneous oscillations of isometric tension (Fig. 10B) and increased CCh-induced isometric force ( $(F_o)_{Test}/(F_o)_{Control} = 167 \pm 11\%$ ,  $n = 8$ ) by 70% ( $p = 0.0009$ ; Fig. 10C). It, however, had no significant effect on the kinetics (Fig. 10D) of the muscarinic

contraction: time-to-peak ( $(t_{\text{peak}})_{\text{Test}}/(t_{\text{peak}})_{\text{Control}}$ ) in control ( $97 \pm 9\%$ ,  $n = 8$ ) and following paxilline treatment ( $104 \pm 7\%$ ,  $n = 8$ ) were not significantly different ( $p = 0.92$ ).

#### 4. Discussion

As an increase of  $[\text{Ca}^{2+}]_i$  is a primary signal for contraction in all types of muscles, the nature of the mechanisms linking excitation to  $[\text{Ca}^{2+}]_i$  mobilisation, as well as the spatial organisation and molecular composition of intracellular  $\text{Ca}^{2+}$  release units are important determinants of the contractile response. However, the mechanisms coupling excitation to  $[\text{Ca}^{2+}]_i$  mobilisation in skeletal, cardiac and smooth muscles are different. While in skeletal muscles membrane depolarization triggers  $\text{Ca}^{2+}$  release from the SR via direct interaction between the voltage sensors in the T-tubules (voltage-gated L-type  $\text{Ca}^{2+}$  channels/the dihydropyridine receptors; VGCCs) and ryanodine receptors (RyRs) expressed in the terminal sacs of the SR (reviewed in [41-43]), in ventricular cardiac muscles  $\text{Ca}^{2+}$  entry through VGCCs triggers RyR-mediated  $\text{Ca}^{2+}$  release via a  $\text{Ca}^{2+}$ -induced  $\text{Ca}^{2+}$ -release (CICR) mechanism (reviewed in [43-47]). In both cases the structural basis for excitation-contraction (E-C) coupling is localisation of the SR RyRs at the ends of sarcomers in close juxtaposition to T-tubular VGCCs.

Cytosolic  $\text{Ca}^{2+}$  which triggers contraction of smooth muscle cells (SMCs) is mobilised either by depolarization of the cell membrane leading to  $\text{Ca}^{2+}$  entry through VGCCs (electromechanical coupling, [1]), or by activation of a variety of receptors (pharmacomechanical coupling, [1]) usually coupled via  $G_{q/11}$ -protein to stimulation of phospholipase C (PLC),  $\text{IP}_3$  production and  $\text{IP}_3$ -mediated  $\text{Ca}^{2+}$  release, or by a combination of these mechanisms. Either of these events, which cause an initial rise in  $[\text{Ca}^{2+}]_i$ , may be further augmented by RyR-mediated  $\text{Ca}^{2+}$  release activated via CICR [5, 8, 16, 20, 34, 48-52]. The relative contribution of RyRs and  $\text{IP}_3$ Rs to intracellular  $[\text{Ca}^{2+}]_i$  mobilisation and the role of these receptors in the genesis of localised  $\text{Ca}^{2+}$ -release events (sparks or puffs), propagating  $\text{Ca}^{2+}$  waves and  $[\text{Ca}^{2+}]_i$  oscillations varies in different types of SMCs, and often depends on the strengths and mechanism of SMC stimulation. In some phasic SMCs, e.g. urinary bladder and vas deferens,  $\text{Ca}^{2+}$  entry through VGCCs is tightly coupled to RyR-mediated  $\text{Ca}^{2+}$  release. Electrical stimulations of these SMCs (under current- or voltage-clamp conditions) triggered an abrupt RyR-mediated  $\text{Ca}^{2+}$ -release at multiple sub-PM regions ('hot spots', [5, 50, 53]). Using 3D-immunofluorescence, freeze fracture and thin section electron microscopy, it was demonstrated that in SMCs of urinary bladder VGCCs and RyRs are in close proximity to each other within the caveolar domains [54], thus forming a complex analogous to  $\text{Ca}^{2+}$  release units of striated muscles [55]. Destruction of caveolae in SMCs of urinary bladder with methyl- $\beta$ -cyclodextrin attenuated coupling between voltage-gated  $\text{Ca}^{2+}$  entry and RyR-mediated  $\text{Ca}^{2+}$  release and reduced contractile responses elicited by electrical stimulation [52]. Nevertheless, it was demonstrated that  $\text{IP}_3$ -mediated  $\text{Ca}^{2+}$ -release is essential for  $[\text{Ca}^{2+}]_i$  mobilisation and contraction, especially (but not exclusively) induced by stimulation of SMCs with neurotransmitters and hormones [19, 20, 30, 33, 34, 56-60]. It therefore was suggested that at least in some SMC types CICR could be initiated and facilitated by  $\text{IP}_3$ -mediated  $\text{Ca}^{2+}$  release [16, 34, 48, 57, 58].

In this study we have demonstrated that strong muscarinic stimulation (with  $10 \mu\text{M}$  CCh) of single ileal SMCs triggers an abrupt sub-PM  $[\text{Ca}^{2+}]_i$  upstroke (SPCU) produced by  $\text{IP}_3$ -mediated  $\text{Ca}^{2+}$  release from sub-PM SR elements. These events were closely associated with action potentials (Fig. 1) and strongly depended on  $\text{Ca}^{2+}$  entry through VGCCs (Figs. 2A and 7), suggesting that in this SMC type E-C coupling involves an initial  $\text{IP}_3$ -mediated  $\text{Ca}^{2+}$  release facilitated by voltage-gated  $\text{Ca}^{2+}$  entry. A molecular basis for this is that  $\text{IP}_3$ Rs in this cell type are expressed in much greater quantity than RyRs (an overall stoichiometric

ratio of RyRs to IP<sub>3</sub>Rs in the guinea-pig intestinal smooth muscle was reported to be 1:9-10 [39]) and are predominantly located in sub-PM SR, while RyRs are mostly confined to the centrally located deep SR (Fig. 8B, [24]), similarly to some other types of phasic SMCs [61]. Differential distribution of RyRs and IP<sub>3</sub>Rs explains the difference between spatio-temporal patterns of Ca<sup>2+</sup> waves induced by direct stimulation of RyRs and Ca<sup>2+</sup> waves triggered following IP<sub>3</sub> mobilisation in response to muscarinic stimulation under conditions when voltage-gated Ca<sup>2+</sup> entry is either facilitated (Fig. 8C and D) or diminished (by holding the cell membrane potential at a negative level [24]).

In gastrointestinal SMCs, a mixed population of muscarinic receptors (M<sub>2</sub> and M<sub>3</sub>) with the predominance of the M<sub>2</sub> subtype (75-82%) are co-expressed (reviewed in [62-64]). There are several signal transduction mechanisms which link activation of these receptors to stimulation of IP<sub>3</sub>R-mediated Ca<sup>2+</sup> release. The main universal Ca<sup>2+</sup> signalling pathway couples activated M<sub>3</sub> receptors via pertussis toxin (PTX)-insensitive G proteins (G<sub>q/11</sub>) to stimulation of phospholipase C β (PLCβ) leading to formation of IP<sub>3</sub> [65, 66]. In addition, activation of M<sub>2</sub> receptors is coupled via PTX-sensitive G proteins (G<sub>i</sub>) to inhibition of adenylyl cyclase activity [63, 66] leading to a decrease in cAMP level and, as a result, to suppression of the inhibitory effects of protein kinase A on the PLCβ – IP<sub>3</sub> – IP<sub>3</sub>R signalling pathway [67, 68]. Finally, activation of muscarinic receptors produces excitation of gastrointestinal (GI) smooth muscles causing depolarization of SMCs and an increase in the frequency of the action potentials via modulation of the activity of many different channel types (reviewed in [64, 69; 70]), of which opening of the cationic channels [35; 71] synergistically regulated via M<sub>2</sub> – G<sub>αo</sub> [37; 72, 73] and/or M<sub>2</sub>/M<sub>3</sub> – G<sub>o</sub> – atypical PLC [64, 74-76] and M<sub>3</sub> – G<sub>q/11</sub> – PLCβ – IP<sub>3</sub> – Ca<sup>2+</sup> [24, 26, 27; 35-37] pathways is one of the major mechanisms of GI smooth muscle excitation. The inward Na<sup>+</sup> current through muscarinic cationic channels (in many smooth muscles, including guinea-pig ileum, these channels have very low, if any, permeability to Ca<sup>2+</sup> [25-27], see also Figs. 3Bc, 4d, and 6Cc) produces membrane depolarization resulting in an increased Ca<sup>2+</sup> influx via VGCCs. There is growing evidence that Ca<sup>2+</sup> entering SMC is “trapped” between the SR and opposed regions of the plasmalemma [59; 77] resulting in an increase of the local [Ca<sup>2+</sup>]<sub>i</sub> up to the order of 10 μM [9, 77]. Using two-photon flash photolysis of “caged” Ca<sup>2+</sup> it was recently demonstrated that a local increase of [Ca<sup>2+</sup>]<sub>i</sub> may trigger IP<sub>3</sub>R-mediated Ca<sup>2+</sup> release [51].

The SPCU triggered by stimulation of SMCs of the guinea pig ileum with 10 μM CCh was virtually abolished by either block of VGCCs (Fig. 3A) or by depletion of intracellular Ca<sup>2+</sup> stores (Fig. 3B). Thus, similarly to Ca<sup>2+</sup> mobilization at sub-PM ‘hot spots’ evoked by electrical stimulation of SMCs from urinary bladder and vas deferens [5, 50, 51, 52], SPCU results from the SR Ca<sup>2+</sup> release induced by Ca<sup>2+</sup> entry (CICR) through VGCCs. After Ca<sup>2+</sup> store depletion the residual CCh-induced [Ca<sup>2+</sup>]<sub>i</sub> transient was spatially uniform, which is characteristic of Ca<sup>2+</sup> entry through VGCCs [8, 50, 59, 77]. Indeed, subsequent inhibition of VGCCs (while keeping Ca<sup>2+</sup> stores depleted) completely abolished [Ca<sup>2+</sup>]<sub>i</sub> mobilisation in response to CCh (Fig. 3B), which also demonstrates that muscarinic cationic channels in SMCs of the guinea-pig ileum are virtually impermeable to Ca<sup>2+</sup> (see also [27]).

In contrast to that reported in SMCs from urinary bladder [50] (where RyRs are predominantly expressed in sub-PM SR elements [53] in close juxtaposition to plasmalemmal VGCCs within multiple caveolar domains [54]), the SPCU in SMCs of the guinea-pig ileum (where sub-PM SR elements are enriched with IP<sub>3</sub>Rs; Fig. 8B and [24]) was not affected by block of RyRs with either 50 – 100 μM tetracaine (Fig. 4) or 100 μM ryanodine (summarised in Fig. 7). Inhibition of RyRs, however, abolished the sustained phase of the CCh-induced [Ca<sup>2+</sup>]<sub>i</sub> transient and/or [Ca<sup>2+</sup>]<sub>i</sub> oscillations (Fig. 4), thus indicating that Ca<sup>2+</sup> release via RyRs (predominantly expressed in centrally located SR in



this cell type; Fig. 8B and [24]) is also involved in CCh-induced  $[Ca^{2+}]_i$  mobilisation. However, in contrast to SMCs from urinary bladder and vas deferens [5, 50, 53], RyR-mediated  $Ca^{2+}$  release in ileal SMCs is 'loosely coupled' [49, 78] to  $Ca^{2+}$  entry through VGCCs. It is also evident that in ileal myocytes  $IP_3Rs$  alone (Fig. 4b) may account for  $Ca^{2+}$  wave propagation, not unlike the situation in guinea-pig colonic myocytes [19].

In contrast with  $Ca^{2+}$  'hot spots' elicited by membrane depolarization in urinary bladder SMCs, which were insensitive to inhibition of  $IP_3Rs$  with 3  $\mu M$  xestospongine C [50], CCh-induced SPCU in ileal myocytes was virtually abolished by inhibition of  $IP_3Rs$  (Figs. 4 and 6B). It should be noted, however, that in both cell types an initial global  $[Ca^{2+}]_i$  transient elicited by muscarinic stimulation was substantially attenuated by  $IP_3R$  inhibition, but only in ileal SMCs this also suppressed the sustained rise of  $[Ca^{2+}]_i$  (Fig. 6C). On the other hand, in ileal SMCs, block of VGCCs or cumulative block of VGCCs and RyRs reduced CCh-induced  $[Ca^{2+}]_i$  transients by 90% (Fig. 7B). Altogether these observations strongly suggest that following muscarinic receptor activation: (1) SPCU results from  $IP_3R$ -mediated  $Ca^{2+}$  release facilitated by  $Ca^{2+}$  entry through VGCCs, (2)  $Ca^{2+}$  mobilised upon initial  $[Ca^{2+}]_i$  transient activates RyRs to release  $Ca^{2+}$  and (3) the sustained rise of  $[Ca^{2+}]_i$  and/or  $[Ca^{2+}]_i$  oscillations are the result of interplay between  $IP_3Rs$  and RyRs.

It should be noted that pharmacological agents used in this study to assess the contribution of  $IP_3Rs$  to SPCU may affect voltage-gated  $Ca^{2+}$  entry induced by muscarinic receptor activation, namely: (1) xestospongine C was shown to inhibit barium current through VGCCs in guinea-pig ileal myocytes but had no effect on  $mI_{cat}$  [79], (2) 2-APB was reported to inhibit  $mI_{cat}$  in SMCs from murine stomach [80]. We found that 2  $\mu M$  xestospongine C inhibited  $I_{Ca}$  by 74% (Fig. 5) and, thus, its effect on muscarinic  $[Ca^{2+}]_i$  mobilisation may partially result from inhibition of VGCCs. Nevertheless, suppression of SPCU by 30  $\mu M$  2-APB, which did not inhibit VGCCs (Fig. 5) and had no effect on CCh-induced membrane depolarization (Fig. 6B), confirms that this event results from  $IP_3R$ -mediated  $Ca^{2+}$  release.

Under conditions when SPCU is abolished (by inhibition of  $IP_3Rs$  or VGCCs), the global  $[Ca^{2+}]_i$  mobilisation within the SMC is substantially attenuated (Fig. 7). It therefore seems likely that SPCU is a key element in the chain of events resulting in the muscarinic contractile response. Indeed, isometric force generated by smooth muscle strips of the longitudinal layer of the guinea-pig ileum in response to 2  $\mu M$  CCh was attenuated by 73% following inhibition of  $IP_3Rs$  (Fig. 9D), similarly to that reported in the guinea-pig distal colon [30]. However, similarly to that reported in urinary bladder, where contraction evoked by electrical stimulation [50] or stimulation of muscarinic receptors [81] was shown to depend on RyR-mediated  $Ca^{2+}$  release activated by CICR, muscarinic contraction of the longitudinal layer of the guinea-pig ileum was attenuated by 70% following inhibition of RyRs (Fig. 9D). This suggests that the sustained phase of the CCh-induced  $[Ca^{2+}]_i$  transient, which depends on RyR-mediated  $Ca^{2+}$ -release (Fig. 4), is crucial for force generation and that the initial  $IP_3R$ -mediated  $Ca^{2+}$  release serves to link  $Ca^{2+}$  entry through VGCCs to RyR-mediated  $Ca^{2+}$  release. It is noteworthy that inhibition of  $IP_3Rs$  also abolished spontaneous oscillations of isometric tension observed in control (Fig. 9B). This indicates that  $IP_3Rs$  are also involved in spontaneous rhythmical contractile activity of gastrointestinal smooth muscles, which is driven by interstitial cells of Cajal (reviewed in [82]). The importance of  $IP_3R$  type 1 for normal activity of gastrointestinal smooth muscles was recently illustrated by the demonstration that gastric smooth muscle from mutant mice lacking the type 1  $IP_3R$  revealed no slow wave activity and had attenuated muscarinic excitatory responses [56].

Another important target for sub-PM  $Ca^{2+}$  mobilisation in SMCs are  $Ca^{2+}$ -sensitive membrane ion channels [8, 9, 11, 33, 83-85]. We have recently demonstrated that  $mI_{cat}$  in

ileal SMCs is synergistically potentiated by  $\text{Ca}^{2+}$  and  $\text{IP}_3$  [24]. Hence, on the one hand, SPCU serves to accelerate membrane depolarization and  $\text{Ca}^{2+}$  influx through VGCCs, thus providing a positive feedback mechanism whereby  $\text{Ca}^{2+}$  entry and  $\text{Ca}^{2+}$  release promote membrane depolarization and further  $\text{Ca}^{2+}$  influx, termed  $\text{Ca}^{2+}$ -induced  $\text{Ca}^{2+}$  entry (CICE) [86]. On the other hand, activation of BK channels by SPCU should limit the rate and the extent of muscarinic excitation. Nevertheless, neither inhibition of  $\text{IP}_3$ Rs with 2-APB (which eliminates SPCU) nor direct inhibition of BK channels with 0.1  $\mu\text{M}$  paxilline accelerated the contractile response to CCh (Figs. 9 and 10). Paxilline (0.1  $\mu\text{M}$ ), however, augmented the muscarinic contractile response by 70% (Fig. 10B and C) but had no effect on tonic tension before CCh application (Fig. 10B). A likely explanation is that  $\text{Ca}^{2+}$  entry through VGCCs facilitated by inhibition of BK channels (via the resulting greater membrane depolarization) does not alter  $[\text{Ca}^{2+}]_i$ , but instead it increases the SR  $\text{Ca}^{2+}$  load, thus causing an increase of CCh-induced isometric force. Thus, it seems likely that overall physiological effect of SPCU is to engage a rapid full-scale  $[\text{Ca}^{2+}]_i$  mobilization, rather than to control contractile activity of intestinal smooth muscles via modulation of the BK channel activity.

In conclusion, SPCU is caused by an abrupt  $\text{IP}_3$ R-mediated  $\text{Ca}^{2+}$  release from sub-PM SR elements facilitated by  $\text{Ca}^{2+}$  influx through VGCCs and serves to augment intracellular  $\text{Ca}^{2+}$  mobilization via CICE (acting on muscarinic cationic channels) and via CICR (acting on RyRs) mechanisms, and represents the key element in the chain of the signalling events in cholinergic contraction.

## Supplementary Material

Refer to Web version on PubMed Central for supplementary material.

## Acknowledgments

Supported by The Wellcome Trust (075112, 074724, 042293) and British Heart Foundation (FS/04/052 and FS/06/077).

## References

1. Somlyo AV, Somlyo AP. Electromechanical and pharmacomechanical coupling in vascular smooth muscle. *J. Pharm. Exp. Ther.* 1968; 159:129–145. [PubMed: 4296170]
2. Navedo MF, Amberg GC, Votaw VS, Santana LF. Constitutively active L-type  $\text{Ca}^{2+}$  channels. *Proc. Natl. Acad. Sci.* 2005; 102:11112–11117. [PubMed: 16040810]
3. Amberg GC, Navedo MF, Nieves-Cintrón M, Molkenkin JD, Santana LF. Calcium sparklets regulate local and global calcium in murine arterial smooth muscle. *J. Physiol.* 2007; 579:187–201. [PubMed: 17158168]
4. Lee CH, Poburko D, Kuo KH, Seow CY, van Breemen C.  $\text{Ca}^{2+}$  oscillations, gradients, and homeostasis in vascular smooth muscle. *Am. J. Physiol.* 2002; 282:H1571–H1583. [PubMed: 11959618]
5. Imaizumi Y, Torii Y, Ohi Y, et al.  $\text{Ca}^{2+}$  images and  $\text{K}^+$  current during depolarization in smooth muscle cells of the guinea-pig vas deferens and urinary bladder. *J. Physiol.* 1998; 510:705–719. [PubMed: 9660887]
6. Bolton TB, Imaizumi Y. Spontaneous transient outward currents in smooth muscle cells. *Cell Calcium.* 1996; 20:141–152. [PubMed: 8889205]
7. Benham CD, Bolton TB. Spontaneous transient outward currents in single visceral and vascular smooth muscle cells of the rabbit. *J. Physiol.* 1986; 381:385–406. [PubMed: 2442353]
8. Bolton TB, Gordienko DV. Confocal imaging of calcium release events in single smooth muscle cells. *Acta Physiologica Scandinavica.* 1998; 164:567–575. [PubMed: 9887979]

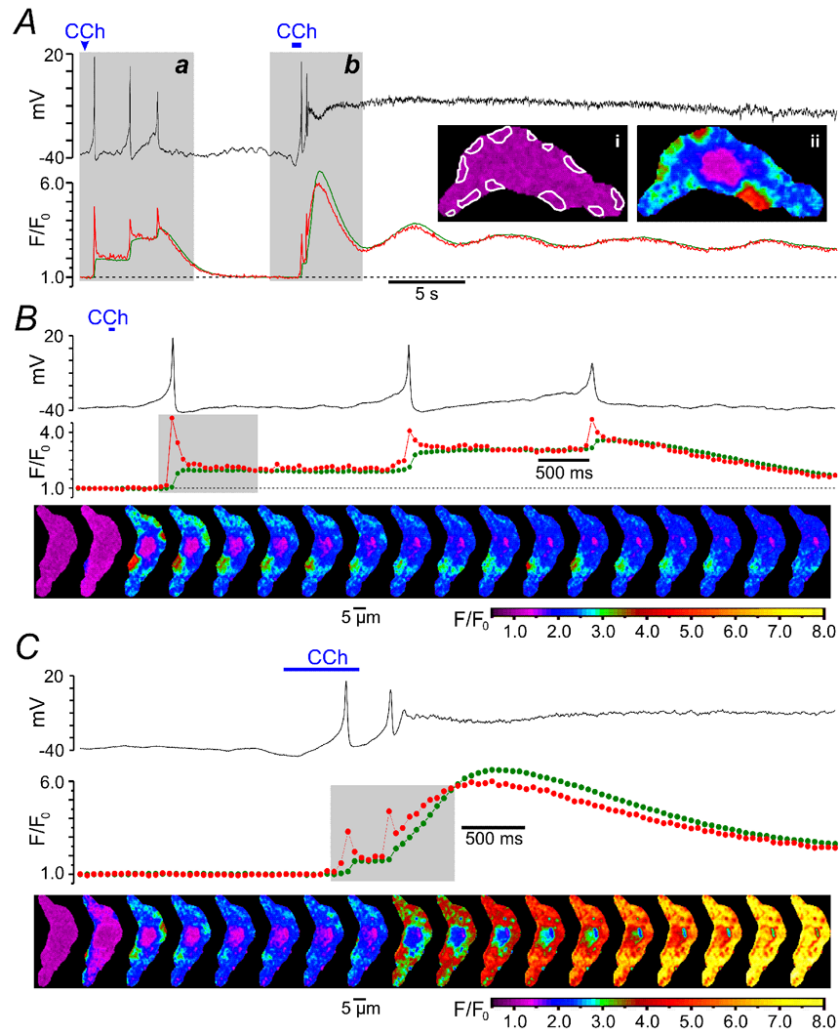
9. ZhuGe R, Fogarty KE, Tuft RA, Walsh JV. Spontaneous outward transient currents arise from microdomains where BK channels are exposed to a mean  $\text{Ca}^{2+}$  concentration on the order of 10  $\mu\text{M}$  during a  $\text{Ca}^{2+}$  spark. *J. Gen. Physiol.* 2002; 120:15–27. [PubMed: 12084772]
10. Cheng H, Lederer WJ, Cannell MB. Calcium sparks: elementary events underlying excitation – contraction coupling in heart muscle. *Science.* 1993; 262:740–744. [PubMed: 8235594]
11. Nelson MT, Cheng H, Rubart M, et al. Relaxation of arterial smooth muscle by calcium sparks. *Science.* 1995; 270:633–637. [PubMed: 7570021]
12. Wier WG, Morgan K.  $\alpha_1$ -adrenergic signalling mechanisms in contraction of resistance arteries. *Rev. Physiol. Biochem. Pharmacol.* 2003; 150:91–139. [PubMed: 12884052]
13. Wellman GC, Nelson MT. Signaling between SR and plasmalemma in smooth muscle: sparks and the activation of  $\text{Ca}^{2+}$ -sensitive ion channels. *Cell Calcium.* 2003; 34:211–229. [PubMed: 12887969]
14. Gordienko DV, Bolton TB, Cannell MB. Variability of spontaneous subcellular calcium release in guinea-pig ileum smooth muscle cells. *J. Physiol.* 1998; 507:707–720. [PubMed: 9508832]
15. Boittin F-X, Coussin F, Macrez N, Mironneau G, Mironneau J. Inositol 1,4,5-trisphosphate and ryanodine-sensitive  $\text{Ca}^{2+}$  release channel-dependent  $\text{Ca}^{2+}$  signalling in rat portal vein. *Cell Calcium.* 1998; 23:303–311. [PubMed: 9681193]
16. Gordienko DV, Bolton TB. Crosstalk between ryanodine receptors and  $\text{IP}_3$  receptors as a factor shaping spontaneous  $\text{Ca}^{2+}$ -release events in rabbit portal vein myocytes. *J. Physiol.* 2002; 542:743–762. [PubMed: 12154176]
17. Bolton TB. Calcium events in smooth muscles and their interstitial cells; physiological roles of sparks. *J. Physiol.* 2006; 570:5–11. [PubMed: 16195319]
18. McCarron JG, Chalmers S, Bradley KN, MacMillan D, Muir TC.  $\text{Ca}^{2+}$  microdomains in smooth muscle. *Cell Calcium.* 2006; 40:461–493. [PubMed: 17069885]
19. MacMillan D, Chalmers S, Muir TC, McCarron JG.  $\text{IP}_3$ -mediated  $\text{Ca}^{2+}$  increases do not involve the ryanodine receptor, but ryanodine receptor antagonists reduce  $\text{IP}_3$ -mediated  $\text{Ca}^{2+}$  increases in guinea-pig colonic smooth muscle. *J. Physiol.* 2005; 569:533–544. [PubMed: 16195318]
20. Lamont C, Wier WG. Different roles of ryanodine receptors and inositol (1,4,5)-trisphosphate receptors in adrenergically stimulated contractions of small arteries. *Am. J. Physiol.* 2004; 287:617–625. [PubMed: 15072954]
21. Gordienko DV, Zholos AV, Bolton TB. Coupling between receptors, channels and intracellular calcium signalling in smooth muscle of small intestine. *J. Physiol.* 2005; 568P:SA2.
22. Mackrill JJ, Challiss RAJ, O'Connell DA, Lai FA, Nahorski SR. Differential expression and regulation of ryanodine receptor and *myo*-inositol 1,4,5-trisphosphate receptor  $\text{Ca}^{2+}$  release channels in mammalian tissues and cell lines. *Biochem. J.* 1997; 327:251–258. [PubMed: 9355760]
23. Taylor CW, Traynor D. Calcium and inositol trisphosphate receptors. *J. Mem. Biol.* 1995; 145:109–118. [PubMed: 7563013]
24. Gordienko DV, Zholos AV. Regulation of muscarinic cationic current in myocytes from guinea-pig ileum by intracellular  $\text{Ca}^{2+}$  release: a central role of inositol 1,4,5-trisphosphate receptors. *Cell Calcium.* 2004; 36:367–386. [PubMed: 15451621]
25. Inoue R, Kitamura K, Kuriyama H. Acetylcholine activates single sodium channels in smooth muscle cells. *Pflügers Arch.* 1987; 410:69–74.
26. Pacaud P, Bolton TB. Relation between muscarinic receptor cationic current and internal calcium in guinea-pig jejunal smooth muscle cells. *J. Physiol.* 1991; 441:477–499. [PubMed: 1667799]
27. Zholos AV, Bolton TB. Effects of divalent cations on muscarinic receptor cationic current in smooth muscle from guinea-pig small intestine. *J. Physiol.* 1995; 486:67–82. [PubMed: 7562645]
28. Brading AF, Sneddon P. Evidence for multiple sources of calcium for activation of the contractile mechanism of guinea-pig taenia coli on stimulation with carbachol. *Br. J. Pharmacol.* 1980; 70:229–240. [PubMed: 7426833]
29. Parekh AB, Brading AF. The sources of calcium for carbachol-induced contraction in the circular smooth muscle of guinea-pig stomach. *Br. J. Pharmacol.* 1991; 104:412–418. [PubMed: 1797308]
30. McCarron JG, Craig JW, Bradley KN, Muir TC. Agonist-induced phasic and tonic responses in smooth muscle are mediated by  $\text{InsP}_3$ . *J. Cell. Sci.* 2002; 115:2207–2218. [PubMed: 11973361]

31. Cheranov SY, Jaggar J. Sarcoplasmic reticulum calcium load regulates rat arterial smooth muscle calcium sparks and transient K<sup>+</sup> Ca currents. *J. Physiol.* 2002; 544:71–84. [PubMed: 12356881]
32. Zheng YM, Wang QS, Rathore R, et al. Type-3 ryanodine receptors mediate hypoxia-, but not neurotransmitter-induced calcium release and contraction in pulmonary artery smooth muscle cells. *J. Gen. Physiol.* 2005; 125:427–440. [PubMed: 15795312]
33. Bayguinov O, Hagen B, Bonev AD, Nelson MT, Sanders KM. Intracellular calcium events activated by ATP in murine colonic myocytes. *Am. J. Physiol.* 2000; 279:C126–C135. [PubMed: 10898724]
34. Zhang WM, Yip KP, Lin MJ, Shimoda LA, Li WH, Sham JS. ET-1 activates Ca<sup>2+</sup> sparks in PASMC: local Ca<sup>2+</sup> signaling between inositol trisphosphate and ryanodine receptors. *Am. J. Physiol.* 2003; 285:L680–L690. [PubMed: 12740215]
35. Benham CD, Bolton TB, Lang RJ. Acetylcholine activates an inward current in single mammalian smooth muscle cells. *Nature.* 1985; 316:345–347. [PubMed: 2410793]
36. Inoue R, Isenberg G. Intracellular calcium ions modulate acetylcholine-induced inward current in guinea-pig ileum. *J. Physiol.* 1990; 424:73–92. [PubMed: 2118179]
37. Wang YX, Fleischmann BK, Kotlikoff MI. M<sub>2</sub> receptor activation of nonselective cation channels in smooth muscles: Calcium and G<sub>i</sub>/G<sub>o</sub> requirements. *Am. J. Physiol.* 1997; 273:C500–C508. [PubMed: 9277347]
38. Gordienko DV, Greenwood IA, Bolton TB. Direct visualization of sarcoplasmic reticulum regions discharging Ca<sup>2+</sup> sparks in vascular myocytes. *Cell Calcium.* 2001; 29:13–28. [PubMed: 11133352]
39. Wibo M, Godfraind T. Comparative localization of inositol 1,4,5-trisphosphate and ryanodine receptors in intestinal smooth muscle: an analytical subfractionation study. *Biochem. J.* 1994; 297:415–423. [PubMed: 8297349]
40. Sanchez M, McManus OB. Paxilline inhibition of the alpha-subunit of the high-conductance calcium-activated potassium channel. *Neuropharmacology.* 1996; 35:963–968. [PubMed: 8938726]
41. Rios E, Stern MD. Calcium in close quarters: microdomain feedback in excitation-contraction coupling and other cell biological phenomena. *Annu. Rev. Biophys. Biomol. Struct.* 1997; 26:47–82. [PubMed: 9241413]
42. Lamb GD. Excitation-contraction coupling and fatigue mechanisms in skeletal muscle: studies with mechanically skinned fibres. *J. Muscle Res. Cell. Motil.* 2002; 23:81–91. [PubMed: 12363289]
43. Dulhunty AF. Excitation-contraction coupling from the 1950s into the new millennium. *Clin. Exp. Pharmacol. Physiol.* 2006; 33:763–772. [PubMed: 16922804]
44. Wier WG, Balke CW. Ca<sup>2+</sup> release mechanisms, Ca<sup>2+</sup> sparks, and local control of excitation-contraction coupling in normal heart muscle. *Circ. Res.* 1999; 85:770–776. [PubMed: 10532944]
45. Cheng H, Wang SQ. Calcium signaling between sarcolemmal calcium channels and ryanodine receptors in heart cells. *Front. Biosci.* 2002; 7:d1867–d1878. [PubMed: 12161336]
46. Soeller C, Cannell MB. Analysing cardiac excitation-contraction coupling with mathematical models of local control. *Prog. Biophys. Mol. Biol.* 2004; 85:141–162. [PubMed: 15142741]
47. Song LS, Guatimosim S, Gomez-Viquez L, et al. Calcium biology of the transverse tubules in heart. *Ann. N. Y. Acad. Sci.* 2005; 1047:99–111. [PubMed: 16093488]
48. White C, McGeown JG. Carbachol triggers RyR-dependent Ca<sup>2+</sup> release via activation of IP<sub>3</sub> receptors in isolated rat gastric myocytes. *J. Physiol.* 2002; 542:725–733. [PubMed: 12154174]
49. Kotlikoff MI. Calcium-induced calcium release in smooth muscle: the case for loose coupling. *Prog. Biophys. Mol. Biol.* 2003; 83:171–191. [PubMed: 12887979]
50. Morimura K, Ohi Y, Yamamura H, Ohya S, Muraki K, Imaizumi Y. Two-step Ca<sup>2+</sup> intracellular release underlies excitation-contraction coupling in mouse urinary bladder myocytes. *Am. J. Physiol.* 2006; 290:C388–C403. [PubMed: 16176965]
51. Ji G, Feldman M, Doran R, Zipfel W, Kotlikoff MI. Ca<sup>2+</sup>-induced Ca<sup>2+</sup> release through localized Ca<sup>2+</sup> uncaging in smooth muscle. *J. Gen. Physiol.* 2006; 127:225–235. [PubMed: 16505145]

52. Hotta S, Yamamura H, Ohya S, Imaizumi Y. Methyl-beta-cyclodextrin prevents  $\text{Ca}^{2+}$ -induced  $\text{Ca}^{2+}$  release in smooth muscle cells of mouse urinary bladder. *J. Pharmacol. Sci.* 2007; 103:121–126. [PubMed: 17202744]
53. Ohi Y, Yamamura H, Nagano N, et al. Local  $\text{Ca}^{2+}$  transients and distribution of BK channels and ryanodine receptors in smooth muscle cells of guinea-pig vas deferens and urinary bladder. *J. Physiol.* 2001; 534:313–326. [PubMed: 11454953]
54. Moore ED, Voigt T, Kobayashi YM, et al. Organization of  $\text{Ca}^{2+}$  release units in excitable smooth muscle of the guinea-pig urinary bladder. *Biophys. J.* 2004; 87:1836–1847. [PubMed: 15345562]
55. Franzini-Armstrong C, Protasi F, Ramesh V. Shape, size, and distribution of  $\text{Ca}^{2+}$  release units and couplons in skeletal and cardiac muscles. *Biophys J.* 1999; 77:1528–1539. [PubMed: 10465763]
56. Suzuki H, Takano H, Yamamoto Y, et al. Properties of gastric smooth muscles obtained from mice which lack inositol trisphosphate receptor. *J. Physiol.* 2000; 525:105–111. [PubMed: 10811729]
57. Boittin FX, Macrez N, Halet G, Mironneau J. Norepinephrine-induced  $\text{Ca}^{2+}$  waves depend on  $\text{InsP}_3$  and ryanodine receptor activation in vascular myocytes. *Am. J. Physiol.* 1999; 277:C139–C151. [PubMed: 10409117]
58. Boittin FX, Coussin F, Morel JL, Halet G, Macrez N, Mironneau J.  $\text{Ca}^{2+}$  signals mediated by  $\text{Ins}(1,4,5)\text{P}_3$ -gated channels in rat ureteric myocytes. *Biochem. J.* 2000; 349:323–332. [PubMed: 10861244]
59. McCarron JG, Bradley KN, MacMillan D, Chalmers S, Muir TC. The sarcoplasmic reticulum,  $\text{Ca}^{2+}$  trapping, and wave mechanisms in smooth muscle. *News Physiol. Sci.* 2004; 19:138–147. [PubMed: 15143210]
60. McCarron JG, MacMillan D, Bradley KN, Chalmers S, Muir TC. Origin and mechanisms of  $\text{Ca}^{2+}$  waves in smooth muscle as revealed by localized photolysis of caged inositol 1,4,5-trisphosphate. *J. Biol. Chem.* 2004; 279:8417–8427. [PubMed: 14660609]
61. Nixon GF, Mignery GA, Somlyo AV. Immunogold localization of inositol 1,4,5-trisphosphate receptors and characterization of ultrastructural features of the sarcoplasmic reticulum in phasic and tonic smooth muscle. *J. Muscle. Res. Cell. Motil.* 1994; 15:682–700. [PubMed: 7706424]
62. Eglén RM, Reddy H, Watson N, Challiss RAJ. Muscarinic acetylcholine receptor subtypes in smooth muscle. *TIPS.* 1994; 15:114–119. [PubMed: 8016895]
63. Gerthoffer WT. Signal-transduction pathways that regulate visceral smooth muscle function. III. Coupling of muscarinic receptors to signaling kinases and effector proteins in gastrointestinal smooth muscles. *Am. J. Physiol.* 2005; 288:G849–G853. [PubMed: 15826932]
64. Zholos AV. Regulation of TRP-like muscarinic cation current in gastrointestinal smooth muscle with special reference to  $\text{PLC}/\text{InsP}_3/\text{Ca}^{2+}$  system. *Acta. Pharmacol. Sin.* 2006; 27:833–842. [PubMed: 16787566]
65. Prestwich SA, Bolton TB. G-protein involvement in muscarinic receptor stimulation of inositol phosphates in longitudinal smooth muscle from small intestine of the guinea-pig. *Br. J. Pharmacol.* 1995; 114:119–126. [PubMed: 7712007]
66. Okamoto H, Prestwich SA, Asai S, Unno T, Bolton TB, Komori S. Muscarinic agonist potencies at three different effector systems linked to the  $\text{M}_2$  or  $\text{M}_3$  receptor in longitudinal smooth muscle of guinea-pig small intestine. *Br. J. Pharmacol.* 2002; 135:1765–1775. [PubMed: 11934818]
67. Zizzo MG, Mule F, Serio R. Mechanisms underlying the inhibitory effects induced by pituitary adenylate cyclase-activating peptide in mouse ileum. *Eur. J. Pharmacol.* 2005; 521:133–138. [PubMed: 16185686]
68. Bai Y, Sanderson MJ. Airway smooth muscle relaxation results from a reduction in the frequency of  $\text{Ca}^{2+}$  oscillations induced by a cAMP-mediated inhibition of the  $\text{IP}_3$  receptor. *Respir. Res.* 2006; 7:34. [PubMed: 16504084]
69. Bolton TB, Prestwich SA, Zholos AV, Gordienko DV. Excitation-contraction coupling in gastrointestinal and other smooth muscles. *Ann. Rev. Physiol.* 1999; 61:85–115. [PubMed: 10099683]
70. Zholos AV. Muscarinic effects on ion channels in smooth muscle cells. *Neurophysiology.* 1999; 31:212–228.
71. Zholos AV, Bolton TB. Muscarinic receptor subtypes controlling the cationic current in guinea-pig ileal smooth muscle. *Br. J. Pharmacol.* 1997; 122:885–893. [PubMed: 9384504]

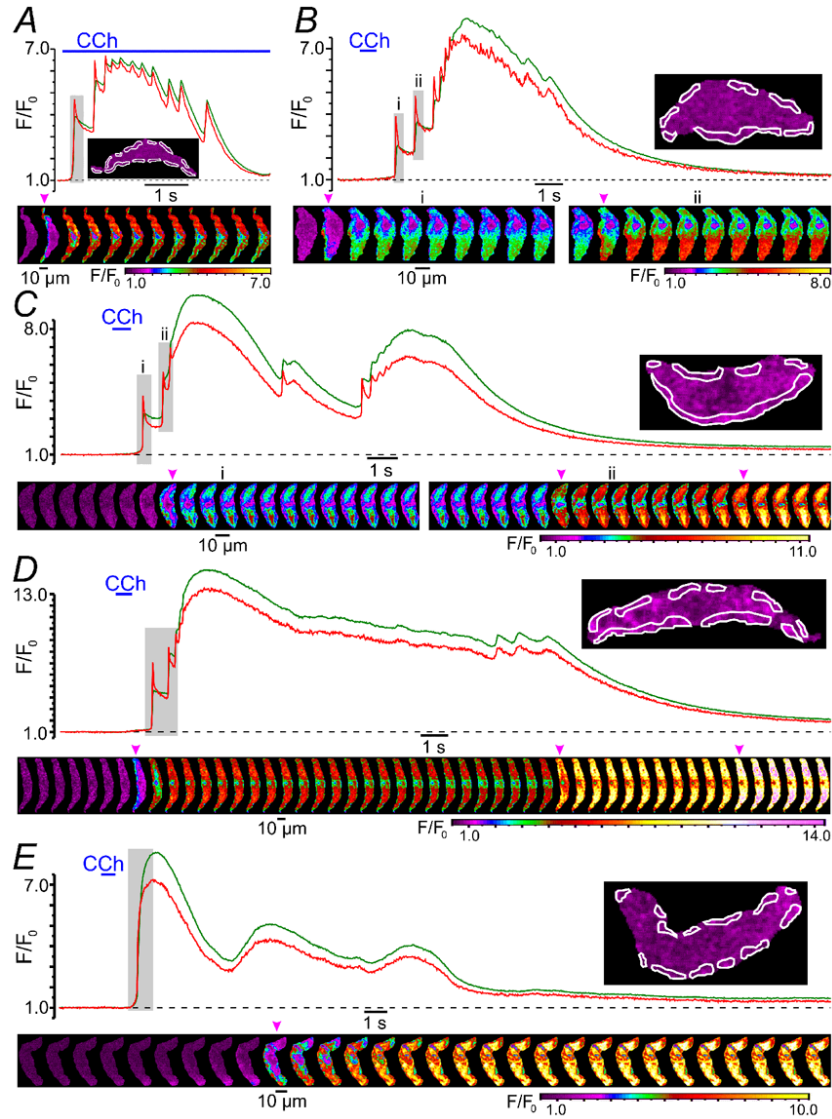


72. Kim YC, Kim SJ, Sim JH, et al. Suppression of the carbachol-activated nonselective cationic current by antibody against  $\alpha$  subunit of  $G_o$  protein in guinea-pig gastric myocytes. *Pflügers Arch.* 1998; 436:494–496.
73. Yan H-D, Okamoto H, Unno T, et al. Effects of G protein-specific antibodies and  $G\beta\gamma$  subunits on the muscarinic receptor-operated cation current in guinea-pig ileal smooth muscle cells. *Br. J. Pharmacol.* 2003; 139:605–615. [PubMed: 12788820]
74. Zholos AV, Tsytsyura Ya.D, Gordienko DV, Tsvilovskyy VV, Bolton TB. Phospholipase C, but not  $InsP_3$  or DAG, dependent activation of the muscarinic receptor-operated cation current in guinea-pig ileal smooth muscle cells. *Br. J. Pharmacol.* 2004; 141:23–36. [PubMed: 14662735]
75. Okamoto H, Unno T, Arima D, et al. Phospholipase C involvement in activation of the muscarinic receptor-operated cationic current in Guinea pig ileal smooth muscle cells. *J. Pharmacol. Sci.* 2004; 95:203–213. [PubMed: 15215645]
76. Unno T, Matsuyama H, Okamoto H, et al. Muscarinic cationic current in gastrointestinal smooth muscles: signal transduction and role in contraction. *Auton. Autacoid. Pharmacol.* 2006; 26:203–217. [PubMed: 16879487]
77. Bradley KN, Craig JW, Muir TC, McCarron JG. The sarcoplasmic reticulum and sarcolemma together form a passive  $Ca^{2+}$  trap in colonic smooth muscle. *Cell Calcium.* 2004;29–41. [PubMed: 15126054]
78. Collier ML, Ji G, Wang Y, Kotlikoff MI. Calcium-induced calcium release in smooth muscle: loose coupling between the action potential and calcium release. *J. Gen. Physiol.* 2000; 115:653–662. [PubMed: 10779321]
79. Ozaki H, Hori M, Kim YS, et al. Inhibitory mechanism of xestospongine-C on contraction and ion channels in the intestinal smooth muscle. *Br. J. Pharmacol.* 2002; 137:1207–1212. [PubMed: 12466229]
80. Lee YM, Kim BJ, Kim HJ, et al. TRPC5 as a candidate for the nonselective cation channel activated by muscarinic stimulation in murine stomach. *Am. J. Physiol.* 2003; 284:G604–G616. [PubMed: 12631560]
81. Rivera L, Brading AF. The role of  $Ca^{2+}$  influx and intracellular  $Ca^{2+}$  release in the muscarinic-mediated contraction of mammalian urinary bladder smooth muscle. *BJU Int.* 2006; 98:868–875. [PubMed: 16978287]
82. Sanders KM, Koh SD, Ward SM. Interstitial cells of cajal as pacemakers in the gastrointestinal tract. *Annu. Rev. Physiol.* 2006; 68:307–343. [PubMed: 16460275]
83. Gordienko DV, Zholos AV, Bolton TB. Membrane ion channels as physiological targets for local  $Ca^{2+}$  signalling. *J. Microsc.* 1999; 196:305–316. [PubMed: 10594771]
84. ZhuGe R, Sims SM, Tuft RA, Fogarty KE, Walsh JV Jr.  $Ca^{2+}$  sparks activate  $K^+$  and  $Cl^-$  channels, resulting in spontaneous transient currents in guinea-pig tracheal myocytes. *J. Physiol.* 1998; 513:711–718. [PubMed: 9824712]
85. Pucovsky V, Bolton TB. Localisation, function and composition of primary  $Ca^{2+}$  spark discharge region in isolated smooth muscle cells from guinea-pig mesenteric arteries. *Cell Calcium.* 2006; 39:113–129. [PubMed: 16297446]
86. Lee HK, Bayguinov O, Sanders KM. Role of nonselective cation current in muscarinic responses of canine colonic muscle. *Am. J. Physiol.* 1993; 265:C1463–C1471. [PubMed: 8279510]

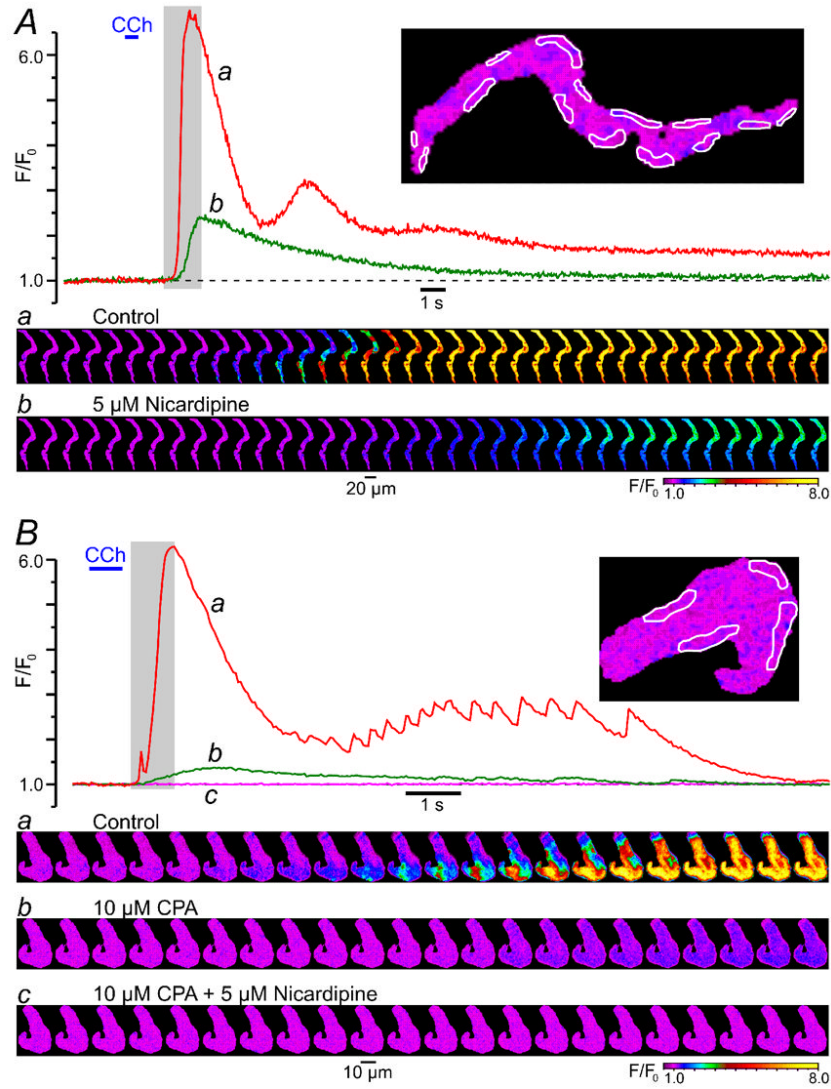


**Fig. 1.**

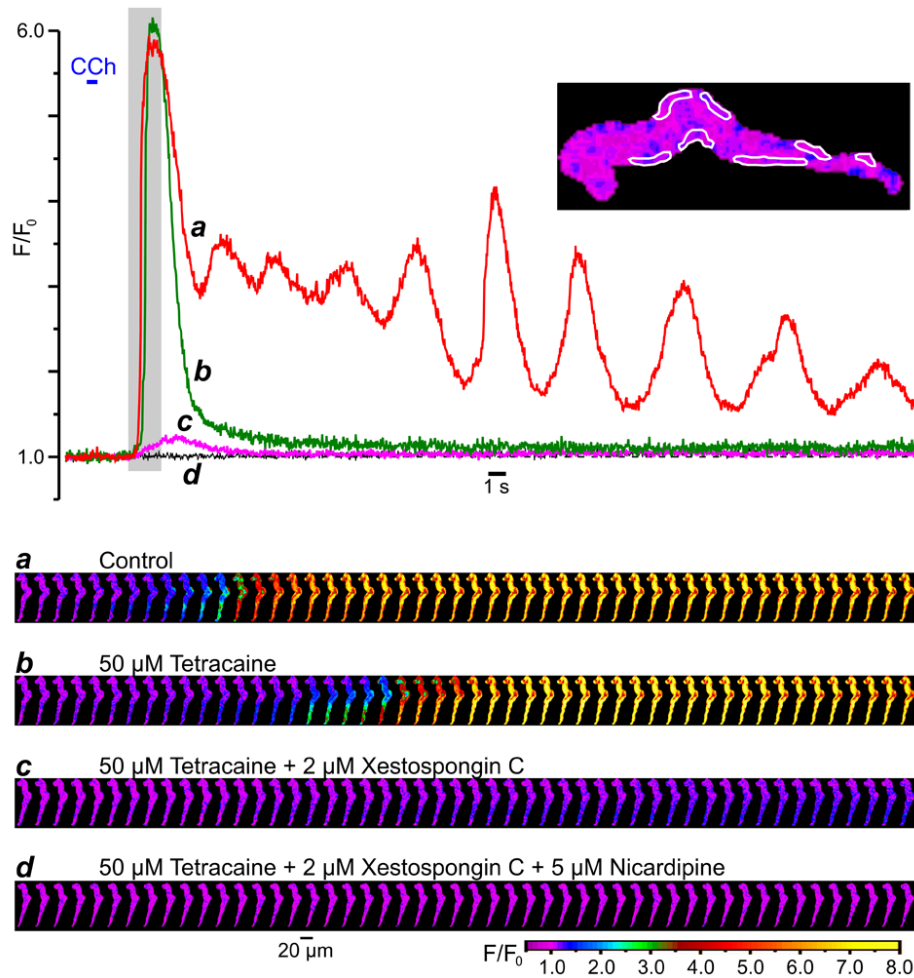
Carbachol (CCh) - induced action potentials are associated with sub-plasmalemmal (sub-PM)  $[Ca^{2+}]_i$  upstroke (SPCU). (A) The record of the cell membrane potential (black trace) is superimposed on the time course of the normalised intensity of fluo-4 fluorescence averaged (red trace) within 12 sub-PM regions outlined in (i) and (green trace) within the total confocal optical slice of SMC. The outlined regions in this and in all subsequent figures were the sites of CCh-induced  $Ca^{2+}$  wave initiation, as illustrated in (ii). The response of the SMC was triggered by  $10 \mu\text{M}$  CCh applied twice from a glass micropipette: as 60-ms pulse (Aa and B) and as 600-ms pulse (Ab and C). The confocal images were acquired 54 ms apart. The fluorescence intensity was normalised to the average fluorescence intensity in a series of images captured before CCh application and colour coded as indicated ( $F/F_0$ ). Two periods of interest highlighted (grey background) in (A) are presented on an expanded time scale in (B) and (C). In (B) and (C) the gallery below the plot shows 18 sequential confocal images (after rotation by  $90^\circ$ ) captured during the period highlighted in the corresponding plot of the normalised fluorescence signal. See also video clips in supplementary material on line.



**Fig. 2.** Spatio-temporal patterns of CCh-induced  $[Ca^{2+}]_i$  transients. The  $x$ - $y$  confocal  $Ca^{2+}$  imaging was performed at 32 Hz (A and B), 40 Hz (C), 44 Hz (D) and 30 Hz (E). For each cell, the time course plot of the normalised fluo-4 fluorescence intensity was averaged (red trace) within sub-PM regions of interest where  $Ca^{2+}$  waves (induced by 10  $\mu$ M CCh) were initiated (insets), and (green trace) within the total confocal optical slice of the SMC. The galleries below the plots show sequential confocal images (after rotation by  $90^\circ$ ) captured during the periods highlighted by grey background in the plots. Magenta arrowheads in the galleries indicate sub-PM  $[Ca^{2+}]_i$  upstrokes.

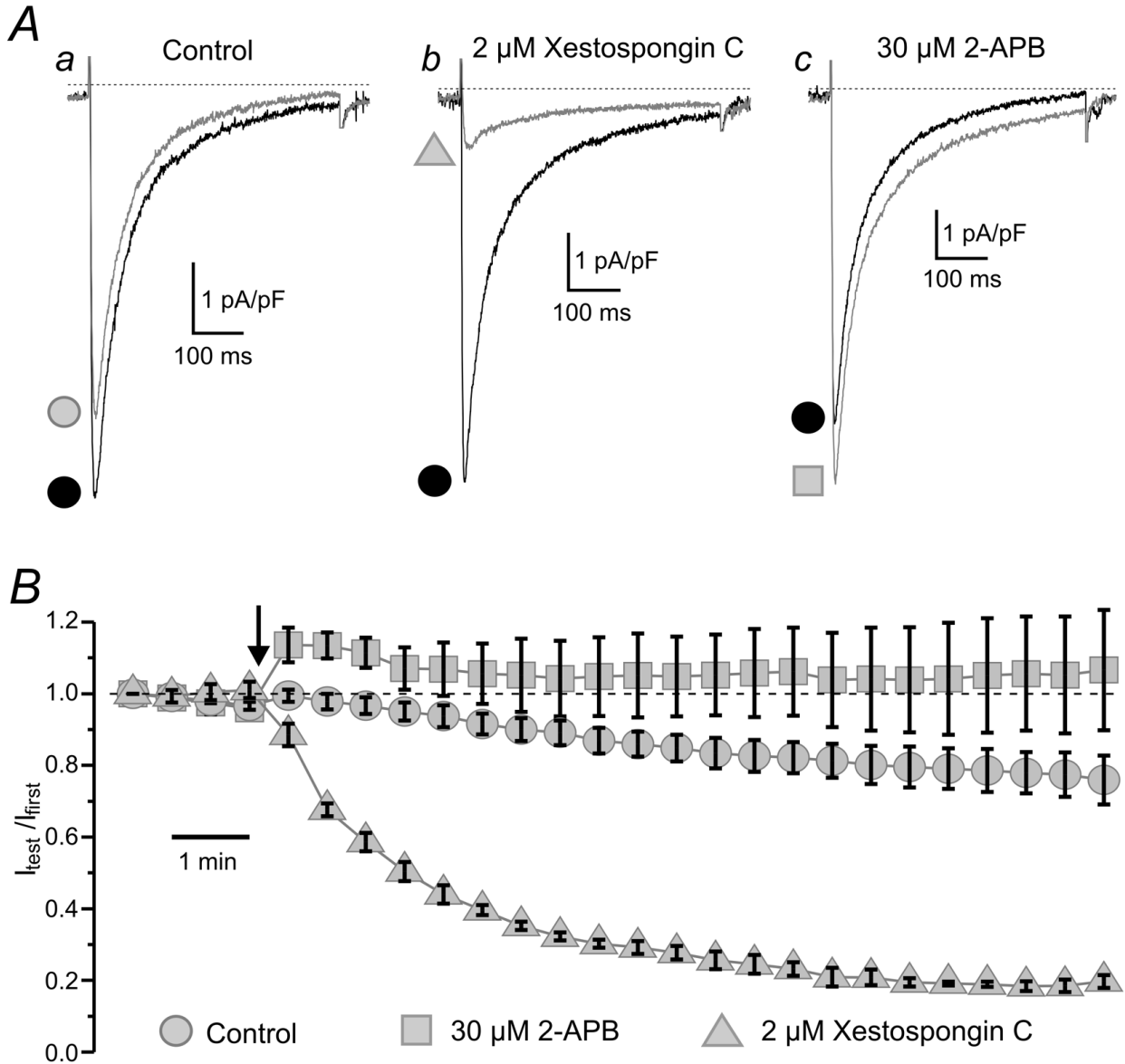


**Fig. 3.** CCh-induced SPCU depends on both voltage-gated  $\text{Ca}^{2+}$  entry and  $\text{Ca}^{2+}$  release from intracellular stores: effect of block of voltage-gated  $\text{Ca}^{2+}$  channels with 5  $\mu\text{M}$  nicardipine (A) and depletion of intracellular  $\text{Ca}^{2+}$  stores with 10  $\mu\text{M}$  CPA (B). The imaging was performed at 26 Hz (A) and 23 Hz (B). The plot shows the time course of the normalised fluo-4 fluorescence intensity averaged within sub-PM regions (outlined) in control (a), after incubation with 5  $\mu\text{M}$  nicardipine or 10  $\mu\text{M}$  CPA (b) and after incubation with 5  $\mu\text{M}$  nicardipine in the presence of 10  $\mu\text{M}$  CPA (c). A 10-min period was allowed between subsequent 600-ms pulses of 10  $\mu\text{M}$  CCh. The galleries below the plots show sequential confocal images (after rotation by 90°) captured during the highlighted periods.



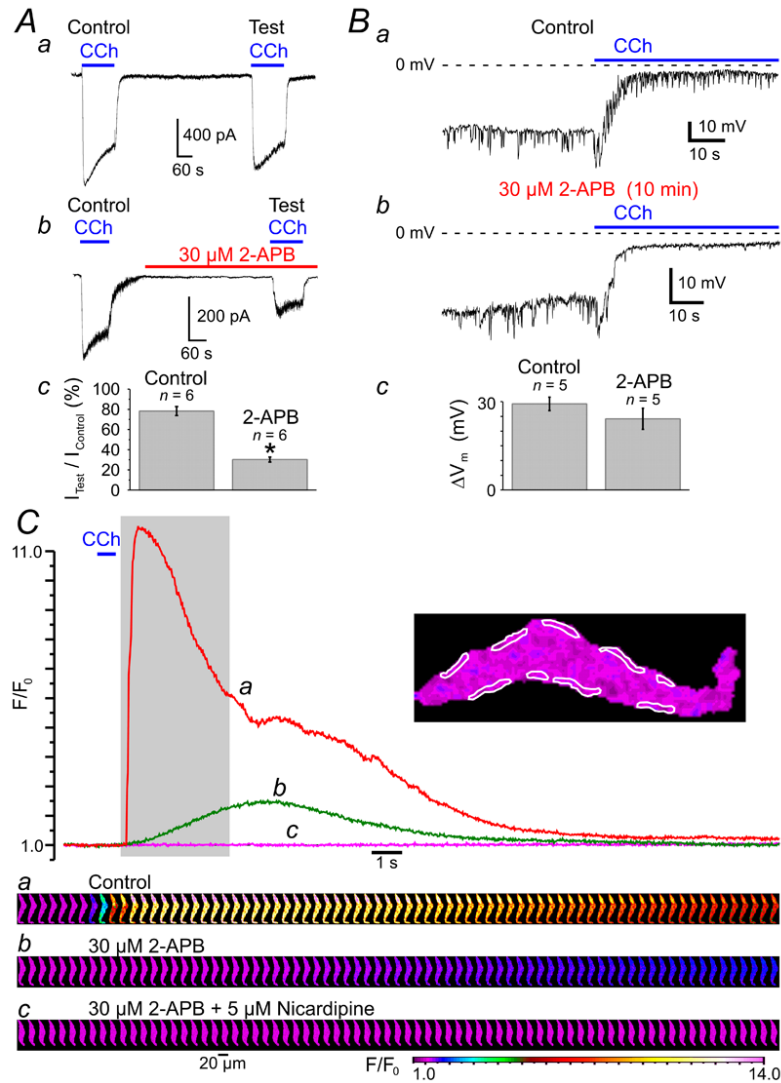
**Fig. 4.** Components of the CCh-induced  $[Ca^{2+}]_i$  transient: successive cumulative inhibitions of RyRs, IP<sub>3</sub>Rs and VGCCs. The fluo-4 loaded SMC was stimulated with 10  $\mu$ M CCh (600-ms pulse) and imaged at 31 Hz. A 10-min period was allowed between CCh pulses. The time course of the normalised fluo-4 fluorescence averaged within seven sub-PM regions (outlined) was plotted in control (a), and following successive cumulative inhibitions by 50  $\mu$ M tetracaine (b), 2  $\mu$ M xestospongine C (c) and 5  $\mu$ M nicardipine (d). The galleries below the plot show sequential images (after rotation by 90°) taken during the highlighted period.



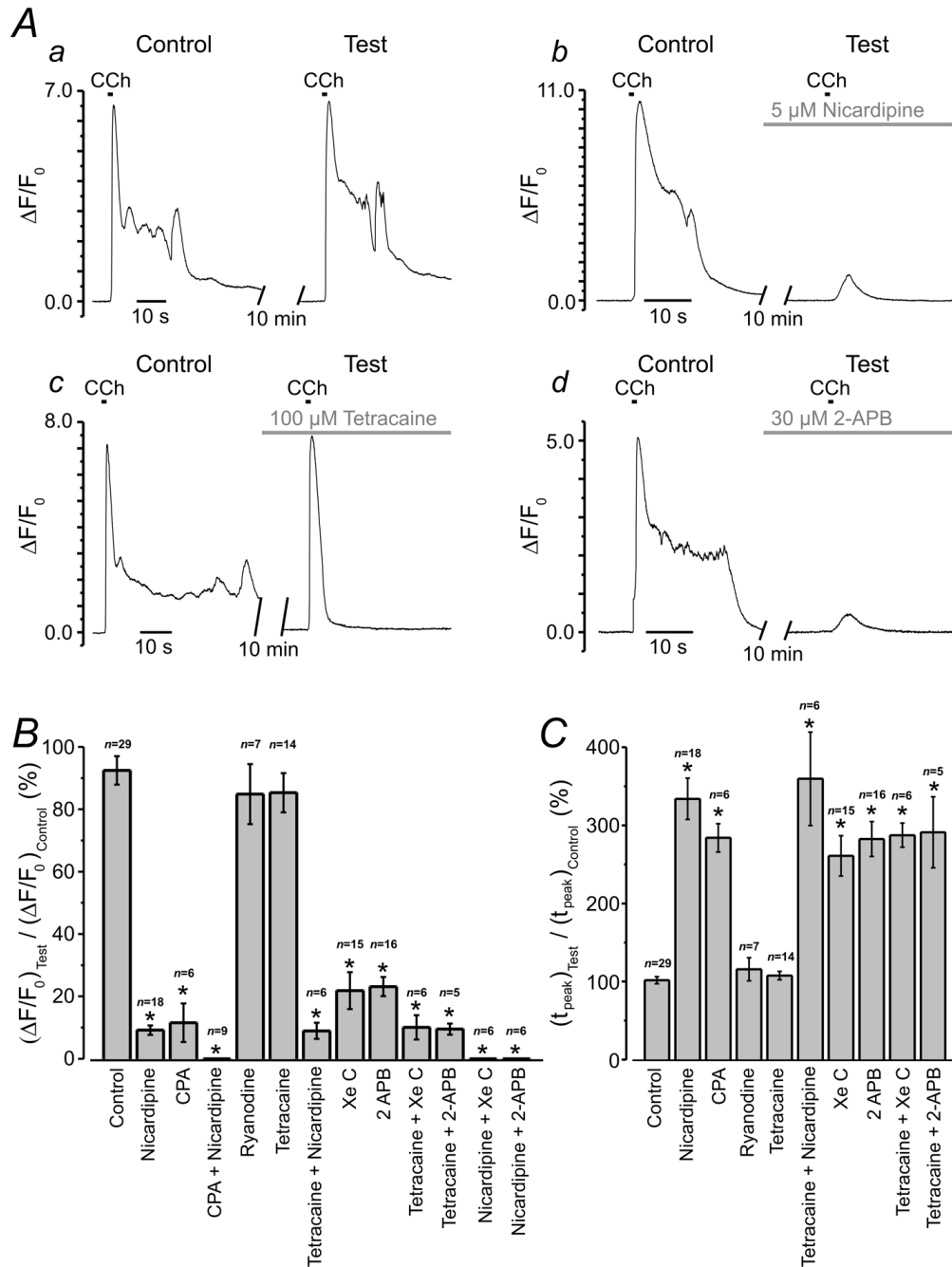


**Fig. 5.**

Effect of xestospongine C and 2-APB on voltage-gated  $\text{Ca}^{2+}$  current ( $I_{\text{Ca}}$ ).  $I_{\text{Ca}}$  was recorded under whole-cell voltage clamp in response to 500-ms steps to 0 mV, applied every 30 s from  $V_h = -80$  mV, in  $\text{Cs}^+/\text{Na}^+$  - containing solutions (see Methods). The traces (A) show  $I_{\text{Ca}}$  evoked by the first step (black) and the step applied 10 min after (grey) in control (a), in 2  $\mu\text{M}$  xestospongine C (b) and in 30  $\mu\text{M}$  2-APB (c). The normalised peak  $I_{\text{Ca}}$  ( $I_{\text{test}}/I_{\text{first}}$ ) is plotted over time (B) in control (circle,  $n = 7$ ), in 2  $\mu\text{M}$  xestospongine C (triangle,  $n = 4$ ) and in 30  $\mu\text{M}$  2-APB (square,  $n = 5$ ). The drug application moment is depicted by the arrow.

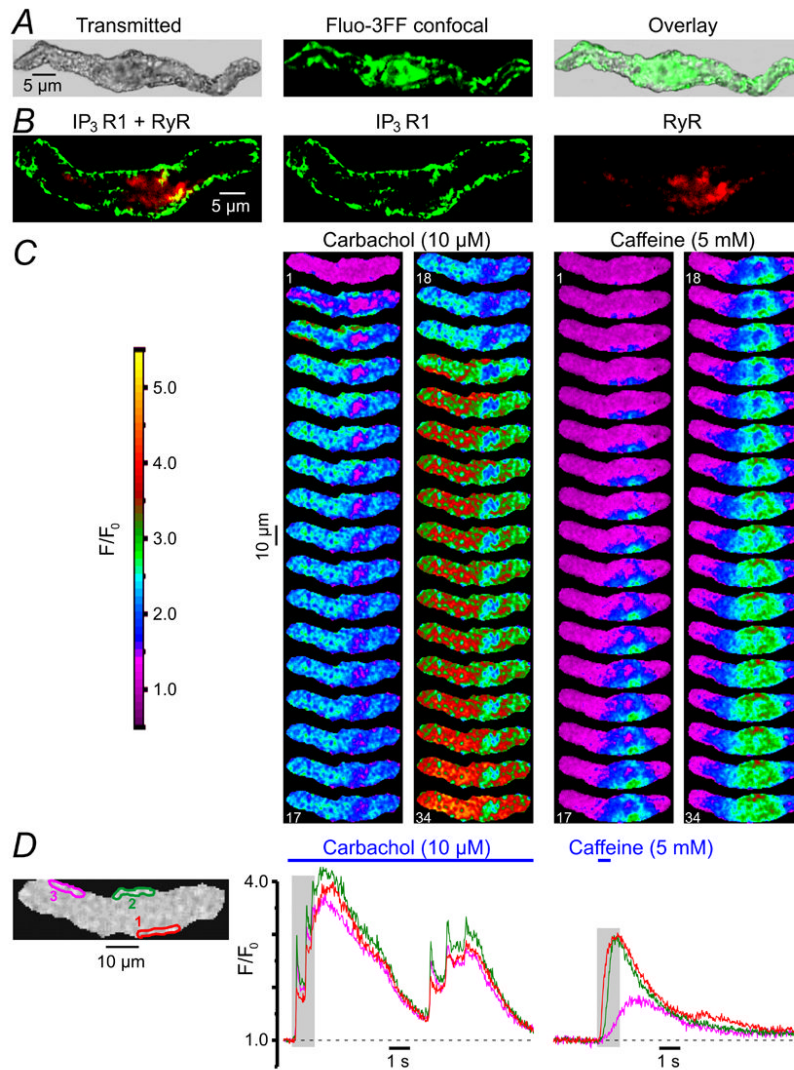
**Fig. 6.**

Effect of 2-APB on (A) muscarinic cationic current ( $mI_{cat}$ ), (B) CCh-induced membrane depolarization and (C) CCh-induced  $[Ca^{2+}]_i$  mobilisation. (A)  $mI_{cat}$  was activated at  $-50$  mV by  $10 \mu$ M CCh in SMC with  $[Ca^{2+}]_i$  clamped at  $100$  nM with  $Ca^{2+}$ /BAPTA buffer and was recorded in  $Cs^+$ -containing solutions (see Methods). Peak  $mI_{cat}$  (a) triggered by the second CCh application (Test) was related to that triggered by the first CCh application (Control).  $30 \mu$ M 2-APB reduced the peak  $mI_{cat}$  (b) on average ( $n = 6$ ) by  $61.5\%$  (c). \*Significant difference ( $p < 0.0002$ ) between control and 2-APB. Application of  $10 \mu$ M CCh depolarized the cell membrane from  $-33 \pm 2$  mV to  $-4 \pm 1$  mV in control (Ba) and from  $-29 \pm 4$  mV to  $-5 \pm 1$  mV ( $n = 5$ ) in  $30 \mu$ M 2-APB (Bb). Summarised in (Bc). The fluo-4-loaded SMC was stimulated with 600-ms pulses of  $10 \mu$ M CCh at 10-min intervals and imaged at 39 Hz (C). The time course of the normalised fluo-4 fluorescence averaged within nine sub-PM regions (outlined) was plotted in control (a), after incubation with  $30 \mu$ M 2-APB (b) and after incubation with  $5 \mu$ M nicardipine in the presence of  $30 \mu$ M 2-APB (c). The galleries below the plot show sequential images (after rotation by  $90^\circ$ ) taken during the period highlighted in the plot.

**Fig. 7.**

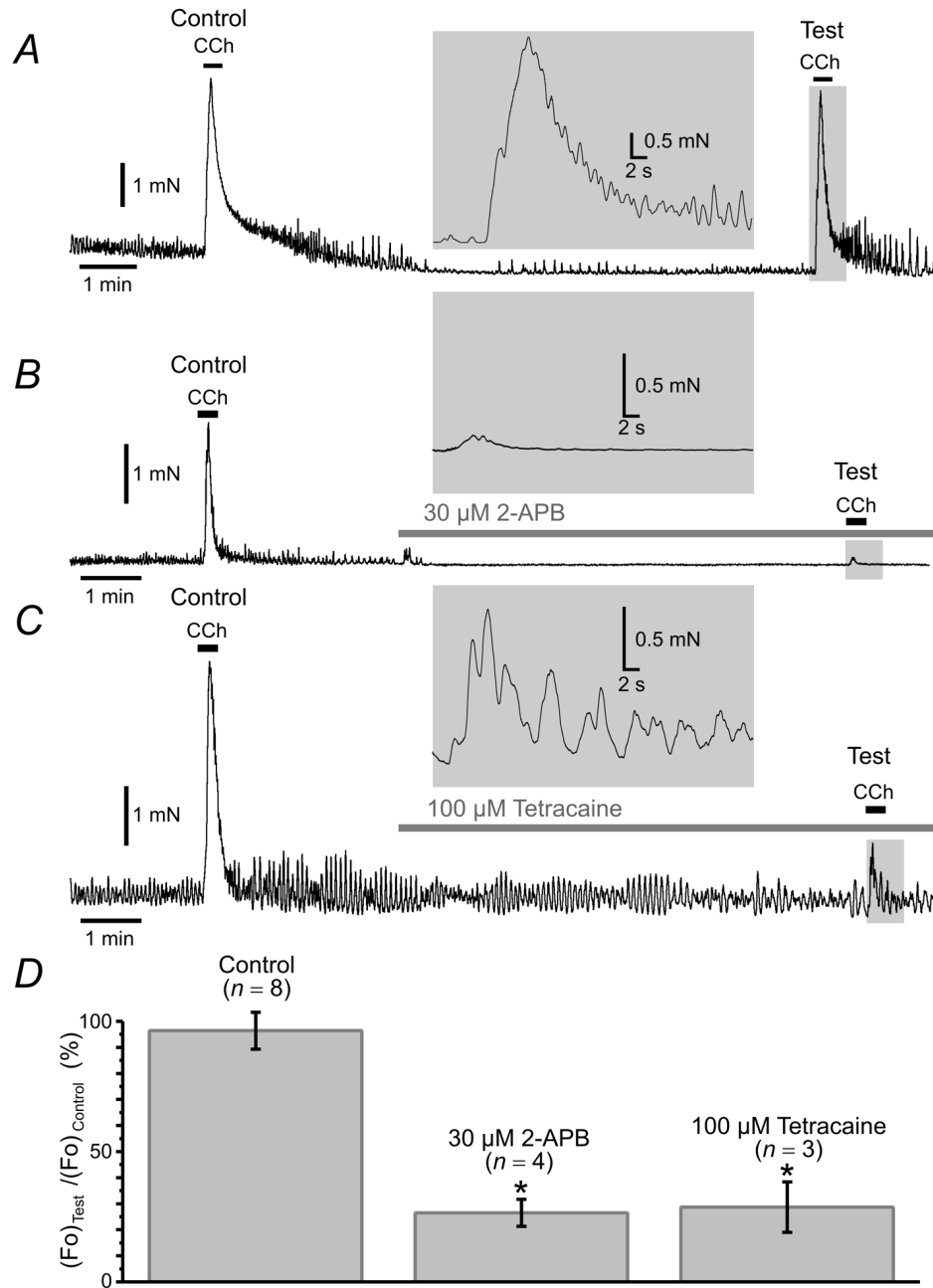
Summary of the effects of VGCC/SERCA/RyR/IP<sub>3</sub>R inhibitors on the initial phase of CCh-induced [Ca<sup>2+</sup>]<sub>i</sub> transient. Experimental protocol is illustrated in (A). The fluo-4 loaded SMCs were stimulated with 600-ms pulses of 10  $\mu$ M CCh applied with a 10 min interval. The response ( $\Delta F/F_0$  averaged at multiple sub-PM regions) to the second CCh application (Test) was related to the response to the first CCh application (Control). The Test response was obtained either in the control (a), or following incubation with a drug (b-d) or a combination of several drugs. Two parameters were examined and summarised: (B) relative change in peak amplitude,  $(\Delta F/F_0)_{\text{Test}}/(\Delta F/F_0)_{\text{Control}}$ , and (C) relative change in time-to-

peak,  $(t_{\text{peak}})_{\text{Test}}/(t_{\text{peak}})_{\text{Control}}$ . \*Significant difference ( $p < 0.0000002$ ) between the parameters in control external solution and in the presence of drug (or drug combination), as indicated.



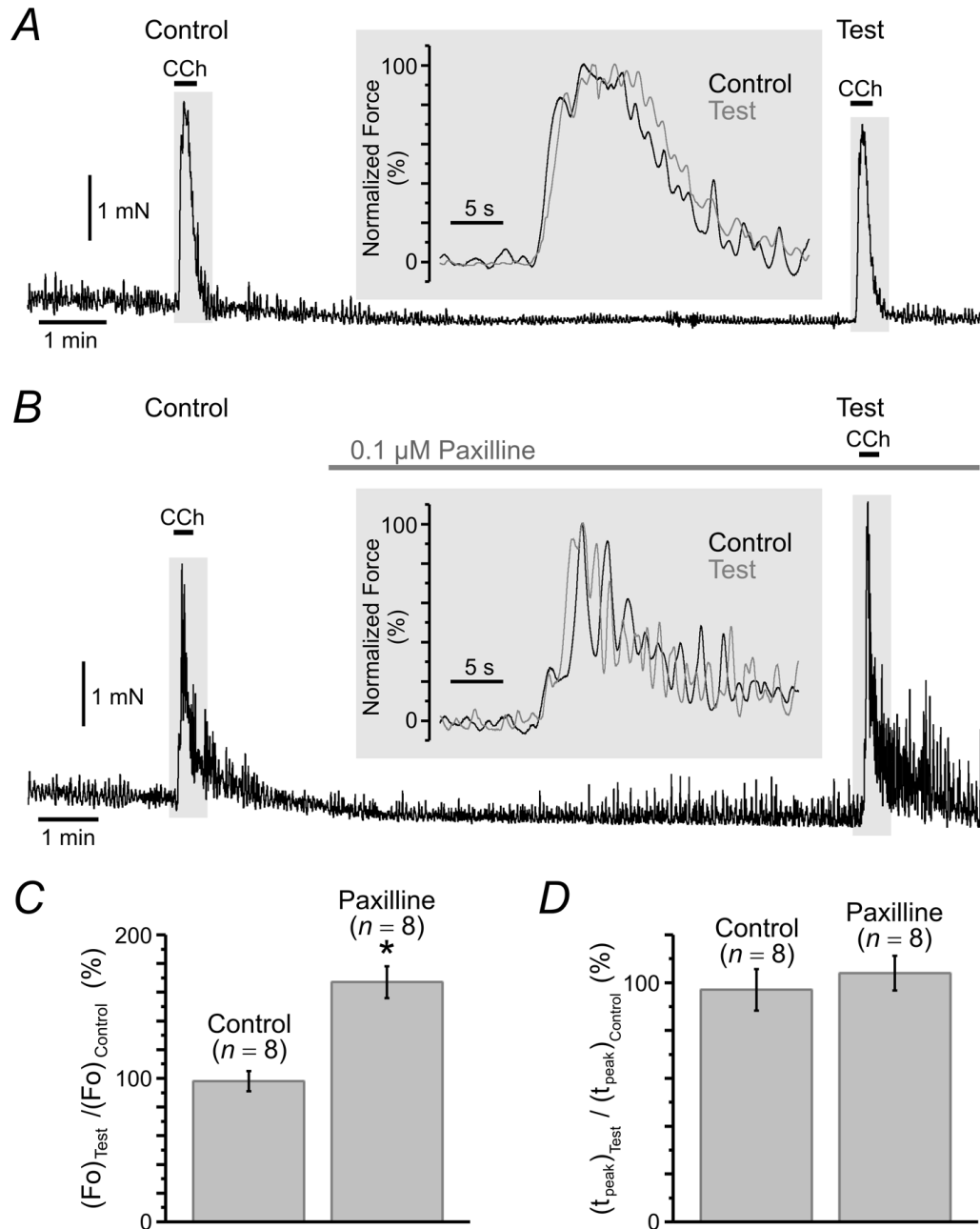
**Fig. 8.** Predominant expression of IP<sub>3</sub>R type 1 in sub-PM SR encourages SPCU. (A) Ca<sup>2+</sup> stores visualised with fluo-3FF consisted of a sub-PM SR network and some central formation. (B) Immunolocalisation of IP<sub>3</sub>R type 1 and RyRs using a double-staining protocol (see Methods). Confocal image of Alexa Fluor 488 fluorescence (green), showing type 1 IP<sub>3</sub>R distribution (middle), and confocal image of Alexa Fluor 633 fluorescence (red), showing RyR distribution (right), are overlaid (left). (C) The fluo-4-loaded SMC was stimulated with 10 μM CCh and 5 mM caffeine (with 10-min interval). Two galleries of images (acquired at 42 Hz) highlight the difference in the initial phase of the responses. (D) The temporal profiles of the fluorescence at three regions outlined in red, green and magenta (left) are shown in corresponding colour.





**Fig. 9.** Effect of inhibition of IP<sub>3</sub>Rs and RyRs on isometric force of muscarinic contraction. Smooth muscle strips from longitudinal layer of the guinea-pig ileum were attached to isometric force transducer at a resting tension load of 5 mN, bathed in the PSS at 37°C and stimulated with 2 μM CCh with a 10-min interval. The response to the second CCh application (Test) was related to the response to the first CCh application (Control). The Test response was obtained in the control (A), in 30 μM 2-APB (B) and in 100 μM tetracaine (C). Insets: the Test responses presented on an expanded time scale. A summary of the relative change in the maximal isometric force ( $(Fo)_{Test}/(Fo)_{Control}$ ) is presented as bar diagram plot (D).

\*Significant difference ( $p < 0.004$ ) between the normalised maximal isometric force in control external solution and in the presence of the drug, as indicated.

**Fig. 10.**

Effect of inhibition of BK channels on isometric force of muscarinic contraction. The protocol was similar to that in Fig.9. The Test response to 2  $\mu$ M CCh was obtained in control (A) and in 0.1  $\mu$ M paxilline (B). Insets: the overlays of Test (black trace) and Control (grey trace) responses normalised to their maximum are presented on an expanded time scale. The bar diagram plots summarise: (C) relative change in the maximal isometric force ( $(Fo)_{Test} / (Fo)_{Control}$ ) and (D) relative change in time-to-peak ( $(t_{peak})_{Test} / (t_{peak})_{Control}$ ). \*Significant ( $p < 0.0008$ ) increase of the maximal cholinergic force following BK channel inhibition was not associated with any significant ( $p = 0.92$ ) change in the kinetics of the contraction.